

2021

An Investigation into the Behaviour of the Magnetic Field from 1 Ga to Present Day

Annalise Cucchiaro

Follow this and additional works at: <https://ro.uow.edu.au/thsci>

University of Wollongong

Copyright Warning

You may print or download ONE copy of this document for the purpose of your own research or study. The University does not authorise you to copy, communicate or otherwise make available electronically to any other person any copyright material contained on this site.

You are reminded of the following: This work is copyright. Apart from any use permitted under the Copyright Act 1968, no part of this work may be reproduced by any process, nor may any other exclusive right be exercised, without the permission of the author. Copyright owners are entitled to take legal action against persons who infringe their copyright. A reproduction of material that is protected by copyright may be a copyright infringement. A court may impose penalties and award damages in relation to offences and infringements relating to copyright material.

Higher penalties may apply, and higher damages may be awarded, for offences and infringements involving the conversion of material into digital or electronic form.

Unless otherwise indicated, the views expressed in this thesis are those of the author and do not necessarily represent the views of the University of Wollongong.

Recommended Citation

Cucchiaro, Annalise, An Investigation into the Behaviour of the Magnetic Field from 1 Ga to Present Day, Bachelor of Science (Honours), School of Earth, Atmospheric and Life Sciences, University of Wollongong, 2021.

<https://ro.uow.edu.au/thsci/187>

An Investigation into the Behaviour of the Magnetic Field from 1 Ga to Present Day

Abstract

The magnetic field of Earth and its behaviour over time is linked to its origin within Earth's liquid outer core. Complex internal processes that operate within the outer core are not only responsible for the creation of the geomagnetic field, but also the magnetic field's strength, stability, and position on Earth. The magnetic field acts as a critical barrier of protection, shielding Earth from harmful solar radiation from the sun and confining Earth's atmosphere beneath the exosphere. As Earth's core evolves and cools over time, it releases heat at the core-mantle boundary (CMB), the magnetic field reflects this evolution by weakening, strengthening, and reversing in polarity over time. It is important to study and form a better understanding of the behaviour of the magnetic field and its intensity over time, as its ability to weaken may give rise to biological and technological damage to Earth and its inhabitants. Variation in magnetic field behaviour over time is preserved in the geologic record, but data is scarce and poorly constrained, thus, numerical modelling solutions remain an essential aspect of paleo-geomagnetic field analysis. In this study, we analyse model-predicted core-mantle boundary heat flux as a proxy indicator of the dynamic evolution of the magnetic field, from 1 Ga to present for four model cases. We do this in aim of including periods known to exhibit the weakening of the magnetic field (superchrons, hyperactive periods and periods of biological extinction), and also investigate the spherical harmonics and Pearson correlation between these data and the current paleo-geomagnetic reversal rate data of two previous studies (Hounslow et al. 2018), Olson et al. 2013). Results conclude that CMB heat flux correlates weakly with the geomagnetic reversal rates, with equatorial CMB heat flux variability (q^* equatorial) correlating the greatest of all quantities investigated. Spherical 3 harmonics analysis reveals a 200 Myr cycle in magnetic field intensity that may correlate with Earth's 200 Myr deep mantle convection cycle.

Degree Type

Thesis

Degree Name

Bachelor of Science (Honours)

Department

School of Earth, Atmospheric and Life Sciences

Advisor(s)

Dr Nicolas Flament

Keywords

Geophysics, Magnetic Field, Mantle Flow

An Investigation into the Behaviour of the Magnetic Field from 1 Ga to Present Day



By:

Annalise Cucchiaro (6089987), Honours Student

School of Earth, Atmospheric and Life Science (SEALS)

University of Wollongong (UOW)

Contact: ac576@uowmail.edu.au

Supervisors:

Dr Nicolas Flament, Senior Lecturer

School of Earth, Atmospheric and Life Sciences

Contact: nflament@uow.edu.au

And

Dr Ömer F. Bodur, Research Fellow

School of Earth, Atmospheric and Life Sciences

Contact: omer@uow.edu.au

Thesis submitted to the department of SEALS, UOW, In partial fulfilment of the requirements for the: Bachelor of Science, Honours Degree

28th of October 2021

Abstract

The magnetic field of Earth and its behaviour over time is linked to its origin within Earth's liquid outer core. Complex internal processes that operate within the outer core are not only responsible for the creation of the geomagnetic field, but also the magnetic field's strength, stability, and position on Earth. The magnetic field acts as a critical barrier of protection, shielding Earth from harmful solar radiation from the sun and confining Earth's atmosphere beneath the exosphere. As Earth's core evolves and cools over time, it releases heat at the core-mantle boundary (CMB), the magnetic field reflects this evolution by weakening, strengthening, and reversing in polarity over time. It is important to study and form a better understanding of the behaviour of the magnetic field and its intensity over time, as its ability to weaken may give rise to biological and technological damage to Earth and its inhabitants. Variation in magnetic field behaviour over time is preserved in the geologic record, but data is scarce and poorly constrained, thus, numerical modelling solutions remain an essential aspect of paleo-geomagnetic field analysis. In this study, we analyse model-predicted core-mantle boundary heat flux as a proxy indicator of the dynamic evolution of the magnetic field, from 1 Ga to present for four model cases. We do this in aim of including periods known to exhibit the weakening of the magnetic field (superchrons, hyperactive periods and periods of biological extinction), and also investigate the spherical harmonics and Pearson correlation between these data and the current paleo-geomagnetic reversal rate data of two previous studies (Hounslow *et al.* 2018), Olson *et al.* 2013). Results conclude that CMB heat flux correlates weakly with the geomagnetic reversal rates, with equatorial CMB heat flux variability (q^* equatorial) correlating the greatest of all quantities investigated. Spherical

harmonics analysis reveals a 200 Myr cycle in magnetic field intensity that may correlate with Earth's 200 Myr deep mantle convection cycle.

Acknowledgements

I extend my deepest thanks to my supervisors Nicolas Flament and Ömer Bodur for the continuous guidance, support, and belief in me throughout past eight months. All the hurdles, walls, and mountains I faced and overcome could not have been possible without you both, and I am deeply thankful for the opportunity and knowledge that I can now take away with me (and share with others!) moving forward; above all I hope to make you both proud!

I thank my family and friends for supporting me and keeping my confidence and drive high through this tough time. In particular I extend thanks to Mark Quoye, a fellow Honours student in the same boat struggling down the same river, for supporting me immensely and remaining a constant reminder of how far we both have come!

I also extend thanks to Andrew Biggin and Christopher Davies, for providing immense amounts of information and advice to Ömer, Nico, and I during this project. The support and ideas you both had provided, instilled excitement and interest in us all, and we are very grateful for this opportunity to collaborate.

Finally, I extend thanks to Kristy Blackburn and coordinators for establishing a safe and informative environment for us Honours students during this difficult time. The effort put toward establishing consistent communication between students and coordinators during lockdown benefited me greatly and I am thankful for the support.

Table of Contents

1	INTRODUCTION	9
1.1	The Geomagnetic Field.....	9
1.1.1	Formation and Role	9
1.2	The Paleomagnetic Record	11
1.2.1	Origin and Record.....	11
1.2.2	Magnetic Reversals and Superchrons	12
1.2.3	Superchrons and Core-Mantle Boundary Heat Flux	14
1.2.4	Basal Mantle Structures	18
1.2.5	Lithospheric Net Rotation.....	21
1.2.6	True Polar Wander.....	21
1.2.7	Dipole Low and a 200 Myr Cycle	23
1.2	The Ediacaran Period.....	24
2	METHODOLOGIES.....	25
2.1	Overview.....	25
2.2	Inputs	26
2.2.1	Tectonic Reconstructions.....	26
2.2.2	CitcomS Mantle Flow	27
2.2.3	Rotations and Corrections.....	28
2.3	Considered Model Cases.....	28
2.3.1	Similarities and Differences.....	28
2.4	Geomagnetic Reversal Rates Used	29
2.5	Computed Quantities	30
2.5.1	The Equatorial Region and LLSVPs.....	30
2.5.2	Total CMB Heat Flux	31
2.5.3	Core-Mantle Boundary Heat Flux Variability (q^*).....	31
2.5.4	Spherical Harmonics Analysis.....	32
2.6	Pearson Correlation.....	34

3	RESULTS.....	36
3.1	Evolution of CMB Heat Flux Through Time	37
3.1.1	Spatial Representation of CMB Heat Flux	37
3.1.2	Numerical Representation CMB Heat Flux	41
3.1.3	Spherical Harmonics of CMB Heat Flux	43
3.2	Evolution of q^* Over Time	45
3.3	Pearson Correlation of Results	47
4	DISCUSSION	49
4.1	Impact of Initial Model Conditions on CMB Heat Flux.....	49
4.1.1	Application of True Polar Wander.....	49
4.1.2	Basal Layer Density	49
4.1.3	Net Rotation	50
4.2	CMB Heat Flux and the Geomagnetic Field Reversal Rate	51
4.3	q^* and the Geomagnetic Field Reversal Rate	51
4.4	The Ediacaran Period and 200 Myr Cycle.....	52
4.4	Limitations	53
5	CONCLUSION	54
6	REFERENCES.....	56
6	APPENDIX	62

List of Figures

I.	Heat Transfer within the Earth and formation of the geomagnetic field [Annalise Cucchiaro, 2021].....	9
II.	Position of ‘normal’ polarity of Earth’s magnetic field [Laura Guerin, CK-12 Foundation].....	10
III.	Magnetic polarity preserved in seafloor on either side of spreading ridge [United States Geological Survey].....	13
IV.	Geomagnetic polarity timescale, reversal rate and the three known superchron periods [Olson, Hinnov & Driscoll, 2014].....	13
V.	Quantities used to define heat flux through a material (shaded region). Source: (Department of Earth, Ocean, and Atmospheric Sciences UBC, 2021).....	15
VI.	Position of the two LLSVPs on Earth (Tuzo and Jason), (Torsvik <i>et al.</i> , 2014).....	18
VII.	Heat transfer within Earth’s Outer Core, CMB, and mantle; as well as mantle structures and their influence upon heat flux at the CMB/convection in the outer core [Dr Nicolas Flament and Annalise Cucchiaro, 2021].....	20
VIII.	Schematic of the three orthogonal axis of inertia on Earth (Steinberger and Torsvik, 2008).....	21
IX.	Schematic representation of TPW driven by mantle convection on a synchronous planet (Leconte, 2018).....	22

X.	Reversal frequency from 600 Ma to present-day. Schematic model of magnetic field behaviour. Source: Meert et al (2016).....	23
XI.	Numerical dynamo reversal frequency and GPTS reversal frequency over time [Olson et al, 2013].....	29
XII.	Average reversal rate of the magnetic field interpolated further back in time [Hounslow et al, 2018].....	30
XIII.	Visualization of spherical harmonics [Becker, W. T, 1997 – 2021].....	33
XIV.	Strength of Pearson's r based upon data relationship. Lund Research.....	33
XV.	Global CMB heat flux from 1 Ga to present-day, in 200 Myr intervals.....	38
XVI.	Global CMB heat flux with TPW and no TPW from 500 Ma to present-day in 100 Myr intervals.....	39-40
XVII.	Total CMB heat flux (both global and equatorial) over time for all models, containing field signal with and without TPW, and all known superchron periods.....	42
XVIII.	Numerical representation of Y00 over time for all models.....	43
XIX.	Numerical representation of degree 2 order 0 over time for all models.....	45
XX.	q^* (both global and equatorial) over time for all models, containing field signal with and without TPW, and all known superchron periods.....	46
XXI.	(a) Average Pearson correlation coefficient of q^* and q_{tot} against both Olson and Hounslow reversal rates, with and without TPW, for all models studied.....	48

List of Tables

I.	Initial conditions used in all models studied (gld 422, 444, 445, 430).....	XXVIII
----	---	--------

1 Introduction

1.1 The Geomagnetic Field

1.1.1 Formation and Role

The geomagnetic field and Earth's magnetosphere play a critical role in protecting all life on earth via reflecting harmful incoming solar radiation from the sun. The geomagnetic field protects the Earth's ozone layer and terrestrial surface from harm, and confines its atmosphere, preventing leakage to space (Wei *et al.*, 2014; Lee *et al.*, 2016). Weakening of the geomagnetic field reduces the intensity of the field and results in greater exposure of Earth's surface to harmful ionising radiation.

Wei *et al.*, (2014) investigated the possible correlation between weakening of the magnetic field, oxygen escape and species extinction. Wei *et al.*, (2014) found that disregarding space weather events such as solar storms and imposing quiet solar-wind conditions, the extreme weakening of the field had the potential to increase oxygen escape rate by 3 - 4 orders of magnitude. During periods of time in which the geomagnetic field is weak, this large increase in oxygen escape rate as a result, would endanger all terrestrial life on Earth.

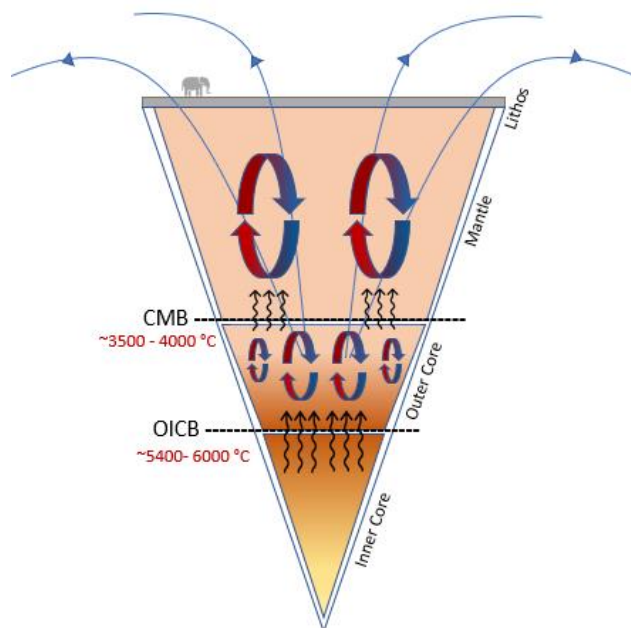


Figure 1. Heat transfer in the Earth's Core and CMB. Small arrows indicate heat transfer via diffusion. Cyclic arrows indicate bulk transfer of heat via convection. Source: Annalise Cucchiaro

The magnetic field of Earth, alike magnetic fields of stars and other planetary bodies, is generated by dynamo action in the liquid metallic outer-core. Dynamo theory refers to the ability of a celestial body to undergo self-sustaining dynamo action and produce a planetary-scale magnetic field on millions to billion-year timescales. In Earth's fluid outer-core, dynamo action is sustained via the complex mechanical fluidic motion of the highly conductive outer-core. This leads to electromagnetic induction, generation of electric currents within the material, and hence the generation of the magnetic field (Fig. 1), (Ojima, Korenaga, & Yin, 2012). This is defined by the Maxwell-Faraday equation, in which spatio-temporal change in an electric field is always followed by a time varying magnetic field (Fleisch, D 2008).

The geomagnetic field itself is structured similarly to a simple dipole field, with its magnetic north pole in the geographic south pole, and its south in the geographic north (Fig. 2).

However, because the field is generated by the complex motion of the liquid outer core (geodynamo action), its recorded intensity and direction over time is correspondingly stochastic and complex (Kutzner and Christensen, 2004; Carbone *et al.*, 2020).

The geomagnetic field is currently in a state of weakening, with the weakest portion of the field spanning across the Atlantic Ocean from

Africa to South America, known as the South Atlantic Anomaly (Terra-Nova, Amit and

Choblet, 2019). This region is growing over time and has advanced westward (Nasuddin et

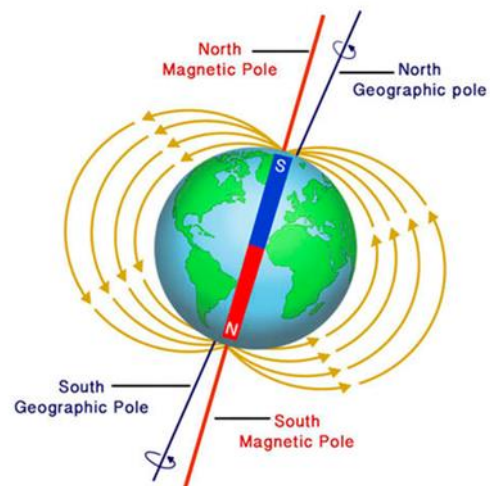


Figure 2. Position of 'normal' polarity of Earth's magnetic field with respect to geographic poles. Source: Laura Guerin, CK-12 Foundation.

al., 2019). Overall, the magnetic field has been decaying at a rate of 5% per century since it was first investigated (Gubbins, Jones and Finlay, 2006).

1.2 The Paleomagnetic Record

1.2.1 Origin and Record

It is impossible to observe the geomagnetic field or inner and outer-core processes with the naked eye. Solving magnetohydrodynamics analytically or through a modelled computational approach using supercomputers to simulate the geodynamo effect remains the most ideal way to observe changing field behaviour with respect to inner and outer-core processes. Despite the field not being physically observable to the naked eye, the geomagnetic field still leaves a paleomagnetic footprint in the ancient geologic rock record.

Ferromagnetic minerals such as iron oxide (magnetite) and nickel present in rocks, magnetize strongly in parallel to the dominant geomagnetic field direction at the current time ('induced magnetization') when the minerals first crystalize; if the field is removed, the rock will still exhibit 'remnant magnetisation' that will be preserved for billions of years.

However, if the rock undergoes circumstances such as metamorphism that place the ferromagnetic minerals above their respective Curie temperature, the magnetization (both 'remnant' and 'induced') is removed entirely (Fowler, C.M.R., 2004).

Magnetization of minerals in ancient rocks whose direction differed from the current field, was first observed by French physicist Achilles Delesse in 1849 – 1850, followed by Bernard Brunhes in 1867–1910, who introduced the possibility that past magnetic field behaviour and hence polarity, was preserved in the rock record. After further investigation into the

magnetization in porcelainites and basalt lava flows, Brunhes discovered samples to exhibit magnetization in the complete opposite direction of the current direction of the field at the time. The possibility for Earth's magnetic polarity to completely 'reverse' was then put forward and explored further throughout the 19th century, and continued to present (Courtillet and Le Mouél, 2007; Seton et al, 2014).

The paleomagnetic record is comprised of all current recorded paleomagnetism in rocks of geologic (igneous and sedimentary) and archeologic origin. Paleomagnetism is best preserved in mid-oceanic spreading ridges (MOR) where new sea-floor is created readily from mantle material. This mantle material can vary in concentration of ferromagnetic minerals depending on the source of the mantle material. Despite the overall composition of the sea floor being mafic, the upper mantle is rather depleted in ferromagnetic minerals, contrasting with the lower mantle, its composition regularly ultramafic and containing a very rich amount of ferromagnetic minerals (Kamenetsky & Maas, 2002).

At the centre of the MOR , when traversing further away perpendicular to the direction of the spreading ridge, the older the sea floor will become and the further back in time we can analyse the history of the geomagnetic field direction and intensity (Fig. 3) over time. Sea floor (from the centre of the ridge onward to subduction zone or continental zone), containing ferromagnetic minerals can be dated, and its age plotted against ferromagnetic mineral direction (or geomagnetic field polarity) at the time, to produce a Geomagnetic Polarity Time Scale (GPTS). Figure 4 displays a portion of the GPTS from 5 Ma to present, with periods of 'reversed' polarity shown in white and periods of 'normal' polarity in black. In this study we use the GTPS as a proxy for geomagnetic field behaviour over time.

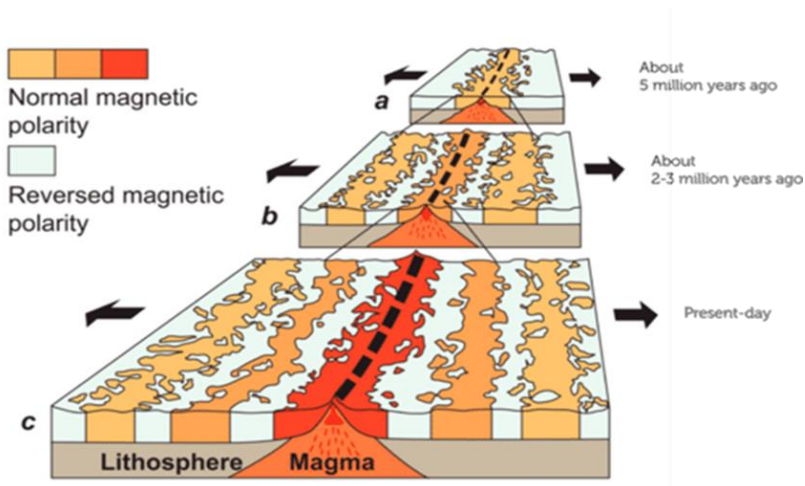


Figure 3. Mid Oceanic Ridge at different ages, displaying the development of magnetic 'stripes' corresponding to changing polarity of the geomagnetic field over time. Varying warm colours depict chrons with respect to the development of the spreading centre. Source: United States Geological Survey. <https://pubs.usgs.gov/gip/dynamic/developing.html>

1.2.2 Magnetic Reversals and Superchrons

Geomagnetic reversal periods occur when the geomagnetic field polarity is re-orientated into a reversed state for long periods of time.

Reversal periods have occurred stochastically over geological timescales and are recorded in the rock record across the entire globe.

The geomagnetic field can also undergo magnetic 'excursions', which unlike reversal periods, demonstrate a change in magnetic field intensity. However, the polar position of the magnetic field itself does not make a full 'reversal' and only varies up to 45° from its original position. In addition to this, magnetic excursions occur on much shorter time scales (1 - 2 Kyr to 10 - 20 Kyr) and do not contain evidence for complete reversal in the geological record across the globe.

The time periods between complete geomagnetic reversal periods are known as 'chrons'.

The duration of chrons fall within a broad range of frequencies that lie between 200 Kyr^{-1} and $> 20 \text{ Myr}^{-1}$. The periods that lie on the upper portion of the spectrum containing low

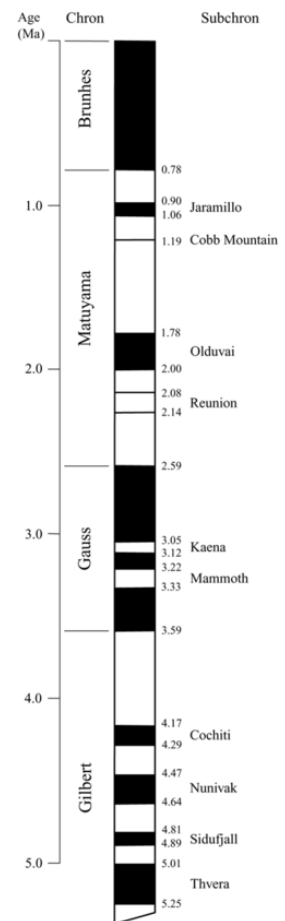


Figure 4. Geomagnetic polarity reversals in the last 5 Ma. Source: United States Geological Survey

reversal rates, are known as ‘superchrons’. Superchrons occur when the magnetic field polar positions remain in a certain position for prolonged timescales; this is true for both ‘normal’ or ‘reversed’ states of polarity. At present, inferred from the current GPTS, there are three superchrons that have been documented since 550 Ma.

The most recent superchron occurred in the Cretaceous from 126 Ma – 84 Ma, lasting 42 Myr in the geomagnetic field ‘normal’ state of polarity. This superchron is better known as the Cretaceous Normal Superchron or CNS (Zhang *et al.*, 2021). The remaining two superchrons occurred in the geomagnetic field ‘reversed’ state of polarity. The first superchron preceding the CNS was the Kiaman Reversed Superchron or KRS which occurred from the mid Carboniferous to mid Permian period (312 – 262 Ma) for 50 Myr (Irving & Parry 1963; Irving & Pullaiah, 1976; Pavlov & Gallet, 2005). The oldest superchron, occurring for 20 Myr from the lower Ordovician to early Silurian period (480 – 460 Ma), known better as the Moyero Reversed Superchron or MRS (Pavlov and Gallet, 2005).

1.2.3 Superchrons and Core-Mantle Boundary Heat Flux

The complex geodynamo of Earth and its magnetic field is impacted by the evolution of Earth’s core over time. The complex convective motion of Earth’s fluid outer core gives rise to the self-sustaining geodynamo and geomagnetic field, thus, studying the causes of change in the intensity and vigour of these convective motions and the amount of heat flux transported to the mantle (Fig. 1), may give insight into the state of the geodynamo and therefore the behaviour of the magnetic field.

Heat flux is defined as the rate at which energy is transferred between two objects and can be used to show the flow direction of heat energy between materials. The unit of heat flux is $\frac{\text{mWatts}}{\text{m}^2}$ and can heat flux be defined by Fourier's Law:

$$q = -\rho c_p k \frac{\Delta T}{\Delta z} \quad \text{or} \quad q = -\rho c_p k \frac{T_2 - T_1}{z_2 - z_1} \quad (\text{Eq. 1, 2})$$

,where q is heat flux, k representing the thermal conductivity of the material, T representing temperature in kelvin, ρ being the density of the material, c_p being the specific heat capacity of the object and z representing distance in meters.

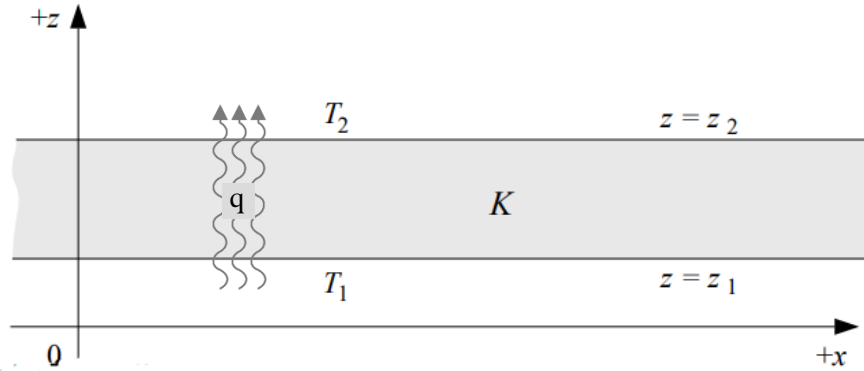


Figure 5. Quantities used to define heat flux through a material (shaded region). Source: (Department of Earth, Ocean, and Atmospheric Sciences UBC, 2021). (Edited).

Therefore, $\frac{\Delta T}{\Delta z}$ denotes the temperature gradient (or change in temperature with distance)

within the boundaries of the region investigated (area between z_2 and z_1) (Fig. 5).

Considering the outer core of Earth is much hotter than the lower mantle, the lower boundary quantities z_1 and T_1 are hotter than the upper boundary quantities z_2 and T_2 , thus, heat flows from the hot body (z_1 and T_1) to the colder body (z_2 and T_2) and is represented by the negative sign at the start of the expression (Equation 1, 2).

An increase in heat flow from the lower boundary or a decrease in temperature at the upper boundary (considering the difference in distance between the two boundaries remain

unchanged) lead to an increase in temperature difference between the two boundaries, an increased temperature gradient of the system, and therefore lead to a higher rate of heat flux within the region. For example, if we consider a cold structure (z_2 and T_2) (such as subducted oceanic material) above the CMB (z_1 and T_1), the cold structure lowers the temperature in its own general region, creating a greater temperature difference between the cold structure and the CMB. This results in an increase in the overall temperature gradient of the region. The temperature gradient of the region in question, is directly proportional to heat flux as shown in Equation 1 and 2; Thus, if the temperature gradient is increased by the cold structure at the CMB, the magnitude of heat flux from the CMB into this cold material will increase to accommodate for the change in temperature. This process occurs inversely for hot structures within the (z_2 and T_2) position above the CMB, as a hotter structure lowers the temperature gradient in the region and suppresses the magnitude of heat flux transported from the CMB to the structure above.

At the core-mantle boundary (CMB), heat transfer from the outer core to the mantle is reflective not only of the convective motions beneath the boundary and all the heat that escapes from the core, but also of the cold and hot structures above it (Nakagawa, 2020). Therefore, heat transfer at the CMB is non-linear, and alike the geomagnetic field, it is inferred from geodynamo models to vary both in space and time. A commonly accepted theory is that the dynamic evolution of the geodynamo is directly linked to CMB heat flux (Driscoll and Olson, 2009; Olson *et al.*, 2010; Carbone *et al.*, 2020; Nakagawa, 2020).

Change in total global CMB heat flux amplitude was investigated by Carbone *et al.*, (2020) by application of empirical mode decomposition of the current GPTS (2012) at the time of publication, and development of a conceptual model in which they used to extract

information on the susceptibility of the GPTS reversal rate caused by changes in the CMB heat flux amplitude. Results revealed that if CMB heat flux varied by a factor of 2 to 3, reversals increase by ~ 10 . This pattern was also reported by Driscoll & Olson, (2011) using purely chemical driven geodynamo simulations, with variation of thermo-chemical CMB buoyancy flux by a factor of 2 increasing reversal rate from $\sim 4.5 \text{ Myr}^{-1}$ to $\sim 1 \text{ Myr}^{-1}$. And additionally, by Olson et al., (2010) when considering topographic forcing of CMB heat flux, an increase in mean amplitude of CMB heat flux by a factor of 2 increased reversal frequency by a factor of 6 to 10.

Global CMB heat flux was considered the best proxy for core evolution and geodynamo/geomagnetic field behaviour, but further study shows that polar regions remain relatively insensitive to CMB heat flux throughout superchrons and periods of magnetic reversals (Olson *et al.*, 2010). More research into equatorial CMB heat flux contribution to magnetic reversals and superchron occurrence has led to the most commonly accepted idea that low Equatorial CMB heat flux induces a slower geomagnetic field reversal rate and therefore promotes field stability (no reversals) for long periods of time, potentially acting as the catalyst for the onset of superchrons.

Glatzmaier et al., (1999) explores CMB heat flux and its influence on reversals by utilizing and comparing eight different 3D numerical simulations of the geodynamo with non-uniform imposed CMB heat flux. Results suggest that the geodynamo was most stable and had lower reversal frequencies, secular variations, and reversal durations when CMB heat flux is axisymmetric and equatorially symmetric, with maximum CMB heat flux in the polar regions and minimum in the equatorial region. This result agrees with low equatorial CMB heat flux providing influence upon field stability and lowering reversal frequency to

promote superchron occurrence. Additionally, Kutzner & Christensen, (2004) also find that virtual geomagnetic pole paths derived from convection-driven 3D numerical geodynamo models show a low-longitudinal bias to the equatorial regions of Earth. A virtual geomagnetic pole path is defined as the location of a magnetic pole on Earth derived from the direction of remnant magnetism within ferromagnetic minerals at a certain place and time. Their findings show that this result is due to the low-latitude regions of high CMB heat flux behaving as centres for magnetic activity and generating intense magnetic flux bundles. They conclude that equatorial heat flux can not only enhance reversal frequency of the geomagnetic field but also suppress reversals entirely based upon the rate of heat flux remaining higher or lower than average.

1.2.4 Basal Mantle Structures

Two large basal mantle structures exist on Earth, sitting just above the CMB within low-latitudinal regions. Basal mantle structures that interact with the CMB may have an influence upon the rate of CMB heat flux transported from the boundary to the mantle. These structures are characteristic of lower-than-average shear wave velocities and remain the largest seismic heterogeneities in the deep mantle. Due to these characteristics their formal

nomenclature is known as Large Low Shear Velocity Provinces or LLSVPs (Su *et al*, 1994).

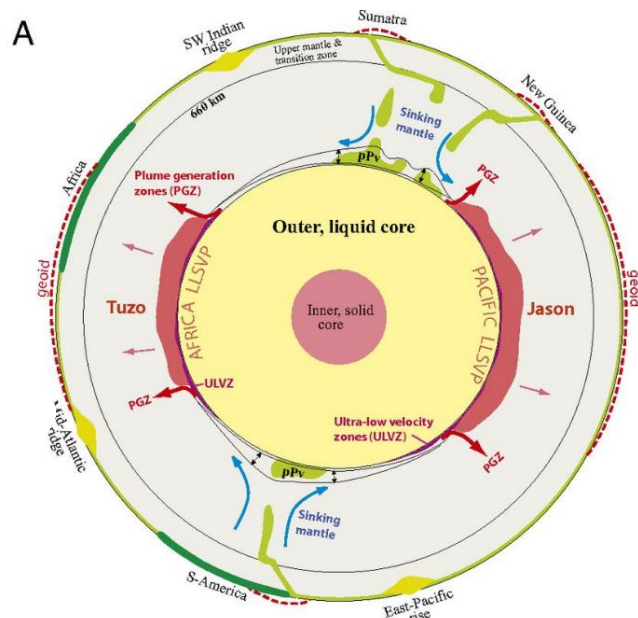


Figure 6. Schematic cross section of the earth from the South Pole region, displaying position of Tuzo and Jason with respect to the inner and surface of Earth. Source: Torsvik *et al*, (2014)

The two LLSVPs extend for thousands of kilometres laterally and vertically, one beneath the Pacific (Jason) and the other beneath Africa (Tuzo) (Fig. 6),(Torsvik *et al.*, 2014).

The exact origin of these structures is still debated, but two commonly accepted hypothesis for their existence and evolution over time (which is debated, (Torsvik *et al.*, 2014; Flament *et al.*, 2017)) remain investigated. The first, states that the structures are remnants of subducted oceanic crust accumulated over the history plate tectonic evolution on Earth (Niu, 2018). And the second, that the structures accumulated from the differentiation and solidification of an ancient basal magma ocean (Garnero, McNamara and Shim, 2016).

The specific temperature and density of the structures are unknown, but are inferred from seismic tomography to be ~ 3000 K (Vilella *et al.*, 2021) and contain a density higher than the surrounding mantle (Li, Zhong and Olson, 2018), acting as a form of heat insulator at the CMB. The temperature gradient at the CMB within these regions become smaller, and thus the resultant heat flux from the outer-core to the mantle becomes suppressed (Fig. 7), this then impacts the vigour of outer-core convection and thus influences the behaviour of the geodynamo (Fig. 1). Inversely, colder material such as subducting oceanic crust interacting with the CMB will in turn increase the temperature gradient and CMB heat flux in the region. This then leads to increasing vigour of convection within the outer-core, leading to increased activity of the geodynamo and geomagnetic reversal rate (Fig. 7) (Li, Zhong and Olson, 2018).

LLSVPs also contain active areas of mantle upwelling on the far edges of the structures known as Plume Generation Zones or PGZ, contributing to generation of Large Igneous Provinces (LIP).

Li et al., (2018) investigates the impact of plume generation at these PGZ and how this may alter LLSVP structure and extent, and potentially alter CMB heat flux within the region.

Thermochemical convection calculations and geodynamic model experiments, show that LLSVP morphology is significantly altered when a plume is first initiated and

ascended and that the local and total heat flux at the CMB during this time is altered.

Additionally, they reveal that LLSVP growth and plume initiation and ascension (in correlation with increased CMB heat flux) evolves over a longer period of time than LLSVP collapse and CMB heat flux to decrease. They suggest that this cycle may be responsible for the reason for a time lag in reversal rate recovery after a superchron, compared to a more sudden change in reversal rate when the superchron is first initiated. They conclude that the resultant variations in CMB heat flux link superchrons with intense pulses of surface vulcanism but the timing between the two phenomena remains troublesome.

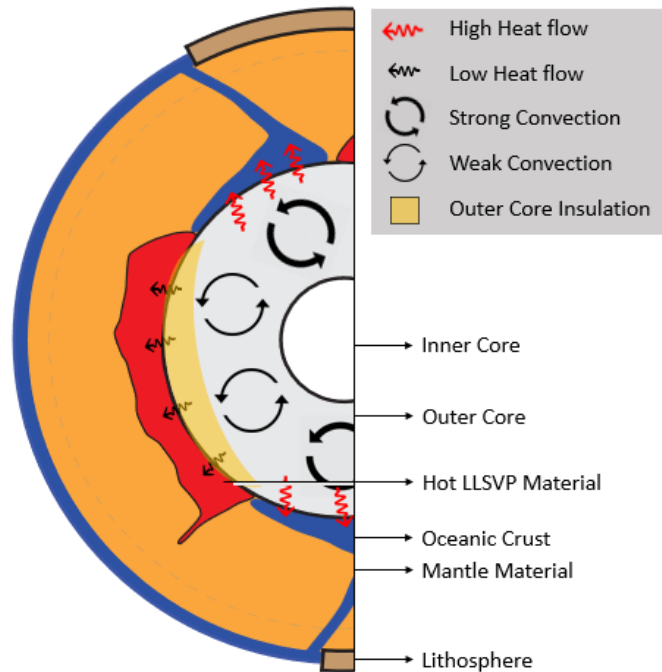


Figure 7. Heat transfer within Earth's Outer Core, CMB, and mantle; as well as mantle structures and their influence upon heat flux at the CMB/convection in the outer core. Source: Nicolas Flament and Annalise Cucchiaro

1.2.5 Lithospheric Net Rotation

Lithospheric net rotation refers to the wholesale motion between the lithosphere and the mantle that arises due to the lateral variations of viscosity structure between the two (toroidal flow) (Rudolph and Zhong, 2014). Lithospheric net rotation forms part of the total past and present tectonic plate motions on Earth, which is reflective of the dynamic evolution of the mantle. Lithospheric net rotation is important to remove from tectonic reconstructions forcing mantle flow models when considering a deep mantle/outer-core reference frame as the dynamic evolution of the outer core itself (and hence the magnetic field) is not directly connected to or reflective of surface tectonics.

1.2.6 True Polar Wander

Earth's physical shape is known as an ellipsoid or geoid. Unlike a sphere, which is symmetrical when dividing in all directions,

the geoid bulges slightly at equatorial regions and is flatter in polar regions. Due to this,

Earth has three orthogonal axis of inertia, the axis with the largest moment of inertia being vertical in line with Earth's spin axis, and the other two of smaller moment of inertia in the horizontal in the equatorial plane (Fig. 8).

When all axis of inertia is in this

position/state, this is referred to as a 'stable' or 'relaxed' state. If the three orthogonal axis of inertia change, then Earth will respond as a

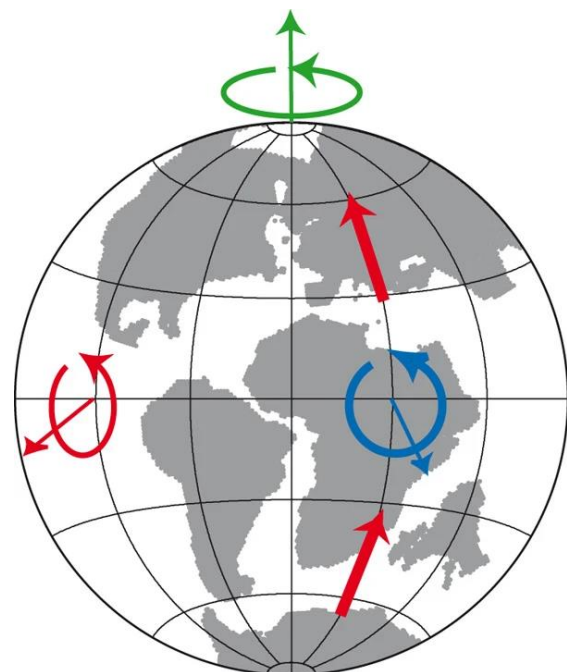


Figure 8. Schematic of the three orthogonal axis of inertia of Earth. Green = Earth spin axis, the largest moment of inertia. Red and Blue = Equatorial points, smaller moments of inertia, blue at centre of continental mass and red exactly 90° away. Source: Steinberger & Torsvik, (2008)

rigid body and rotate to realign the axis with the largest moment of inertia with its own spin axis allowing for Earth to maintain its state of stability (Evans, 2002). However, in doing this, the position of its geographic North and South poles will change respectively, and over longer time scales, exhibit a state of 'wander'. This rotation of Earth in response to a change in maximum moment of inertia is known as True Polar Wander or TPW.

The rate of TPW over time is directly dependent on how fast Earth's geoid changes and how fast the Earth then responds to the change in inertia by adjusting its rotating axis. Earth's geoid structure can change from small (relative to a global scale) to large-scale alterations of Earth's surface by mantle processes. Regions of hot low-density material upwelling either via mantle convection (large scale) or plume ascension above LLSVPs (smaller scale), cause bulging at surface of the equator (positive dynamic topography). Conversely, regions of downwelling such as zones of subduction (smaller scale) or down-going regions of mantle convection (large scale) cause flattening or declination of the polar surface (negative dynamic topography) (Fig. 9).

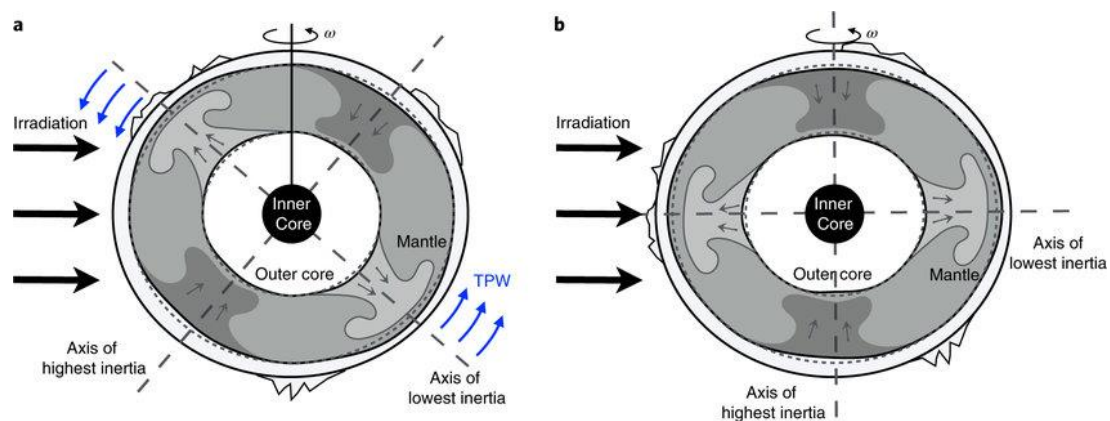


Figure 9. TPW driven by large-scale mantle convection, lighter shaded areas refer to mantle upwellings causing positive anomalies at the surface of the geoid; and darker shaded areas of mantle downwelling, causing negative anomalies at the surface of the geoid. Blue lines show rotation of Earth into a 'stable' state in response to axis' maximum moment of inertia not aligning with Earth's rotational axis. a shows before and b after Earth's response in the form of TPW. Source: Leconte, J, (2018)

Unlike relative plate motions, TPW is a global phenomenon, and considering the geomagnetic field is generated from rotationally induced excitations of the outer core, during a TPW event, Earth's magnetic poles remain aligned with Earth's rotation axis and follow the axis as it shifts to adjust for this change in inertia. Ultimately, it is appropriate that the reference frame used for paleomagnetic data is corrected for TPW.

1.2.7 Dipole Low and a 200 Myr Cycle

Dipole lows are representative of time periods in which the geomagnetic field is

experiencing very low field strength

intensities. Recent studies hypothesise

that the geomagnetic field alternates

between dipole lows and superchrons

over Earth's history, and that this cycle

is reflective of deep Earth processes and

mantle convection cycles (Biggin *et al.*,

2012). Shallow mantle convection cycles

occur on ~50 Myr time periods, whereas

deep mantle convection cycles operate

in ~200 Myr time periods (Zhong and

Zhang, 2005). Two dipole lows were

present prior to the onset of both

Cretaceous Normal and Kiaman

Reverse superchrons (Fig. 10), known

as the Mesozoic dipole low and mid-

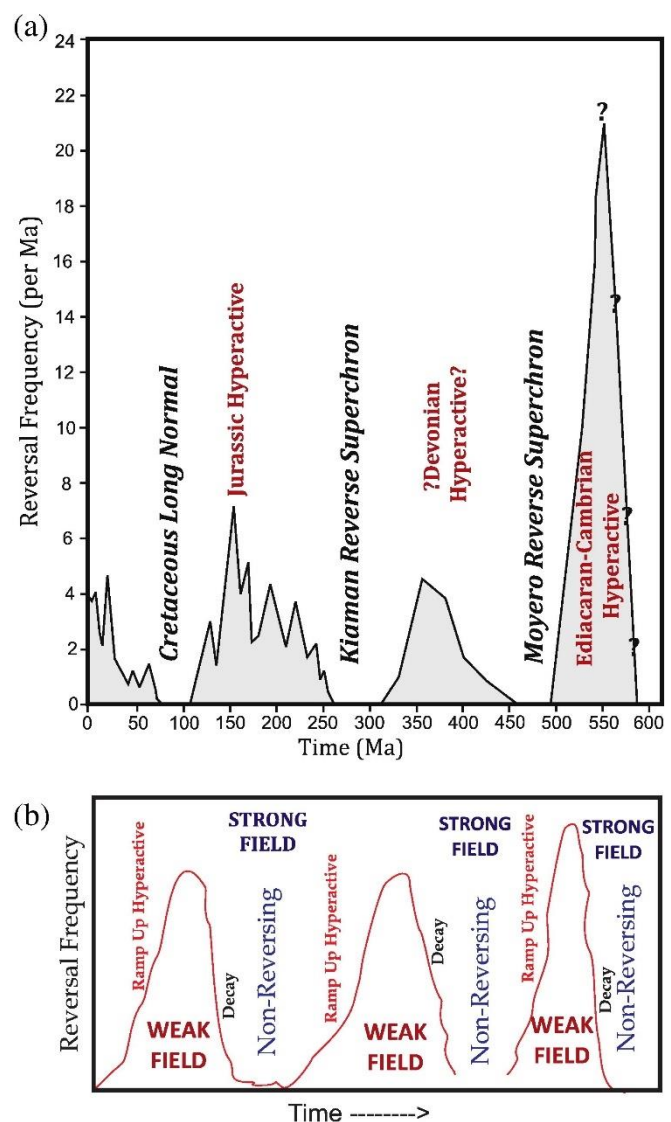


Figure 10) (a) Reversal frequency from 600 Ma to present-day. (b) Schematic model of magnetic field behaviour. Source: Meert *et al* (2016)

Palaeozoic dipole low respectfully (Meert *et al.*, 2016; Hawkins *et al.*, 2021). The dipole lows occurred from 80-85 Myr before each superchron onset, establishing a possible 200 Myr cycle between dipole low and superchrons. We explore the idea of a 200 Myr cycle in geomagnetic field intensity over time during our analysis of CMB heat flux magnitude and variability over time.

1.2 The Ediacaran Period

When the geomagnetic field is rapidly reversing, the magnetic field becomes weak. In turn, the role of the magnetic field in deflecting harmful radiation from the sun is compromised to a certain extent, allowing for both the penetration of harmful radiation into Earth's atmosphere and land surfaces, as well as the escape of oxygen from the ozone layer causing permanent damage to Earth's protective absorption layer (Wei *et al.*, 2014; Lee *et al.*, 2016). A famous extinction event known as the 'End-Ediacaran Extinction' (EEE) was documented at ~540 Ma during rapid reversal activity of the geomagnetic field (Meert *et al.*, 2016; Thallner, Biggin and Halls, 2021).

The geomagnetic reversal rate at the EEE was so large that geological evidence of TPW is sparse and confusing, making it difficult to link CMB heat flux change, the reversal rate of the field and the positioning/movement of the poles (Robert, Greff-Lefftz and Besse, 2018).

In addition to this, studies suggest that the Ediacaran period marks the start of Earth's inner core growth although its age is highly debated. If Earth's core started growing during this period it would support the occurrence of rapid and stochastic reversals of the geomagnetic field as the convective regime present during dynamo action within the core would be disturbed (Bono *et al.*, 2019). When the inner core grows, iron within the core freezes and

produces latent heat that is used to power the geodynamo, as the core dynamically evolves further, all heat lost from the core during evolution is expelled at the CMB, to the mantle; CMB heat flux and its evolution over time, is crucial to analyse in order to understand the evolution of the core and how it impacts the intensity of the geomagnetic field. Derived from zircon data, the presence of the geomagnetic field of Earth extends back to as old as 4.2 Ga (Tarduno *et al*, 2015), whereas data from extant rocks dictate the age of the field to be ~3.45 Ga (Tarduno *et al*, 2010).

We analyse the evolution of CMB heat flux during the timing of the Ediacaran and EEE, as well as consider the possibility of inner core growth at this time.

2 Methodologies

2.1 Overview

This study involved analysing the numerical output of CMB heat flux from CitcomS mantle flow simulations across four models from 1 Ga to present-day in 20 Myr increments. Each model case had different input basal layer densities preceding simulation, contributing to differing CMB heat flux spatially and in intensity as a result. Tectonic reconstructions were used to force mantle flow simulations, and a TPW correction was applied to these reconstructions for the purpose of comparison to paleomagnetic data. CMB heat flux was analysed via defining a series of quantities and comparing these graphically over time with paleomagnetic reversal rates from two studies (Olson *et al.*, 2013; Hounslow *et al.*, 2018). CMB heat flux signal was also decomposed into spherical harmonics to investigate the spatial change of heat flux over time, with particular focus on a degree two order zero

structure (Y_0^2) to study equatorial heat flux change over time. Pearson correlation was also carried out for all quantities defined in analysis, both with and without an imposed rolling average on CMB heat flux data. All numerical calculations, as well as map, graph, and data synthesis were carried out using PyGMT and other packages within the programming language Python.

2.2 Inputs

2.2.1 Tectonic Reconstructions

Tectonic Reconstructions are used to force mantle flow in CitcomS simulations. Imposing accurate and high-resolution tectonic coupling within a mantle flow simulation is computationally expensive, thus, a semi-empirical approach developed by Bower *et al*, (2015) known as the “progressive data assimilation method” is used within the models considered. This method allows for the simulation of mantle flow regimes associated with specific tectonic conditions and environments occurring on Earth today.

Plate tectonic boundary conditions within these reconstructions must be updated in relatively short increments of time to avoid inaccuracies in tectonic plate placements that can affect the positioning and progression of subduction zones and spreading ridges, impacting mantle evolution over time. The plate tectonic reconstruction used within this project is derived from a recent study by (Merdith *et al.*, 2021), reconstructing past tectonic history of the Neoproterozoic to present day in 20 Myr intervals of time.

2.2.2 *CitcomS* Mantle Flow

CitcomS is a finite element code designed to solve incompressible or compressible convection within a spherical shell. Simulated mantle flow in *CitcomS* is time dependent and evolves whilst actively solving for mass, momentum, and conservation of energy within the system over time. The simulation of mantle flow evolves over time, the tectonic reconstruction imposed upon the spherical shell's surface 'forces' mantle flow within the shell. The *CitcomS* code evolves by first solving for conservation of momentum, providing bulk velocities of mantle material movement, and then further with consideration of advection and diffusion of heat during this process. *CitcomS* then solves for both variable viscosity. Earth's mantle is approximated to act as a Newtonian fluid, in which viscosity varies with both temperature and depth; variations in viscosity is limited to three orders of magnitude within *CitcomS* mantle flow simulation, however, lateral variations in viscosity expected to occur within the solid Earth exist in orders of magnitude far higher than what is computationally possible.

The initial condition of each modelled case also includes a basal layer that lies just above the CMB, this layer is compositionally distinct from the surrounding mantle. The density (compared to the surrounding mantle) and nature of the basal layer varies between each modelled case investigated within this project. The *CitcomS* simulation output for each modelled case was provided at the start of the project, in the form of global grid files at 20 Myr intervals containing the temperature at 2840 km depth (later calculated into heat flux for analysis).

2.2.3 Rotations and Corrections

Predicted CMB heat flux variations over time across all modelled cases studied here, are analysed with and without TPW correction applied. Current reconstructions of TPW that we utilise in this project, extend back to 520 Ma (Torsvik *et al.*, 2012, 2014), which remains a limitation to the correction. TPW correction was applied to the global *CitcomS* predicted CMB heat flux grid for each case, in the form of a rotation file containing rotations specific to the Torsvik *et al.*, (2012/2014) studies. This was carried out within Python using PyGPlates and other Python tools.

2.3 Considered Model Cases

1.3.1 Similarities and Differences

Net rotation was removed from the *CitcomS* output grids in consideration for the reference frame of Earth's core. This was done for modelled Cases 1,2 and 3; Case 4 was left unaltered to allow for a strict assessment of the impact Net rotation has on influencing outer-core processes. Case 2 is the model that is closest to the conditions that are characteristic of the deep Earth based upon seismic tomography.

Table 1) Input parameters varied across mantle flow models

Modelled Case	Basal Layer Density (%) in Comparison with the Ambient Mantle	Net Rotation Removed
Case 1	Same as the ambient mantle	Yes
Case 2	+1%	Yes
Case 3	+2%	Yes
Case 4	+1%	No

1.4 Geomagnetic Reversal Rates

The two geomagnetic reversal rates considered in analysis are derived from Olson *et al.*, (2013) and Hounslow *et al.* (2018). Olson *et al.* (2013) included the current geological GPTS record (and its reversal frequency) at the time, which contained missing data between 440 – 360 Ma (Fig. 11). Hounslow *et al.* (2018) attempted to fill in the gaps of missing data during the Palaeozoic by use of linear interpolation in an age versus log (GPTS reversal rate) space, to reflect the normal distribution of the GPTS reversal rate (Fig. 12). They applied this interpolation under the general assumption that the GPTS reversal rate activity differs during superchron periods and periods of normal reversal behaviour.

Geomagnetic field reversal rates are the primary quantity in which CMB heat flux is compared and analysed against within this project. The Hounslow *et al.* (2018) model-corrected reversal rate was provided in 10 Myr increments by Dr. Andrew Biggin. CMB heat flux data was up-sampled from 20 Myr to 10 Myr increments using python and pandas tools in order to remain at the same temporal resolution. The reversal rate data of Olson *et al.* (2013) were digitized from Figure 11 and sampled in 10 Myr increments for consistency with the Hounslow *et al.* (2018) analysis and CMB heat flux data.

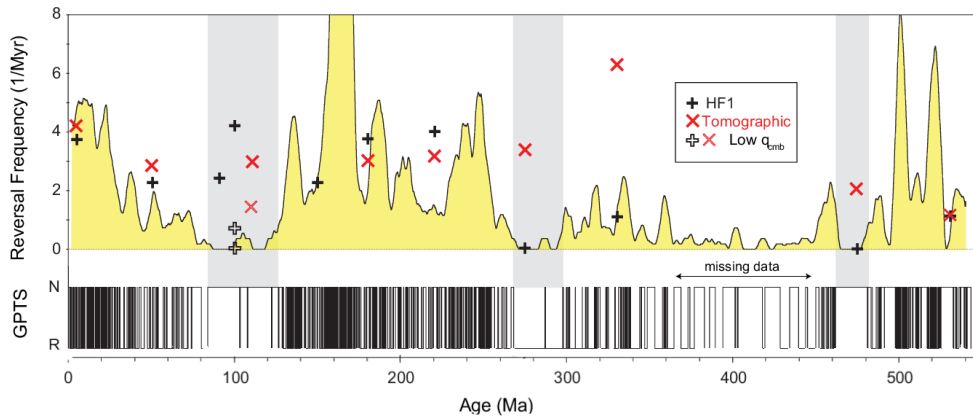


Figure 11) Current GPTS (bottom panel) with geomagnetic reversal rate filled in yellow (top panel). Grey shaded areas correspond to the three known superchron events. Symbols in key refer to Olson *et al.* (2013) numerical dynamo reversal frequencies. Source: Olson *et al.* (2013) (Edited).

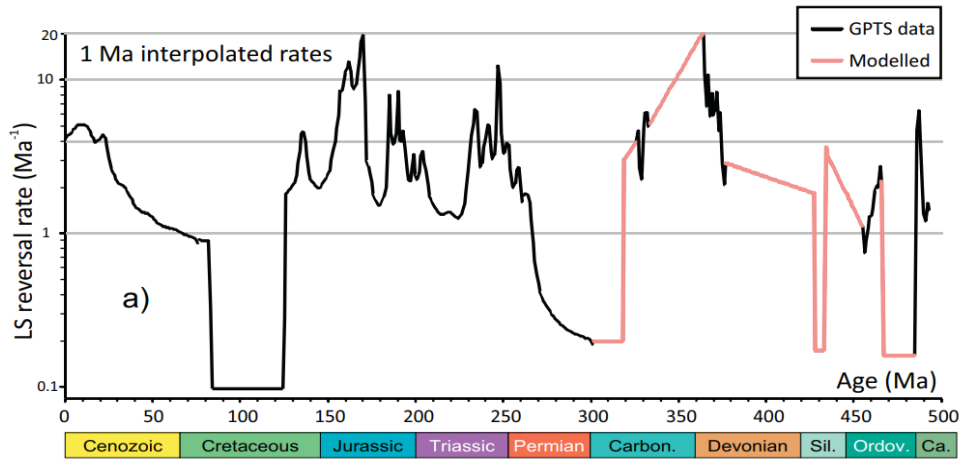


Figure 12) Geomagnetic reversal rate from geological GPTS data (solid black curves) and from linear interpolation (solid beige curves) over time. Source: Hounslow et al (2018).

1.5 Computed Quantities

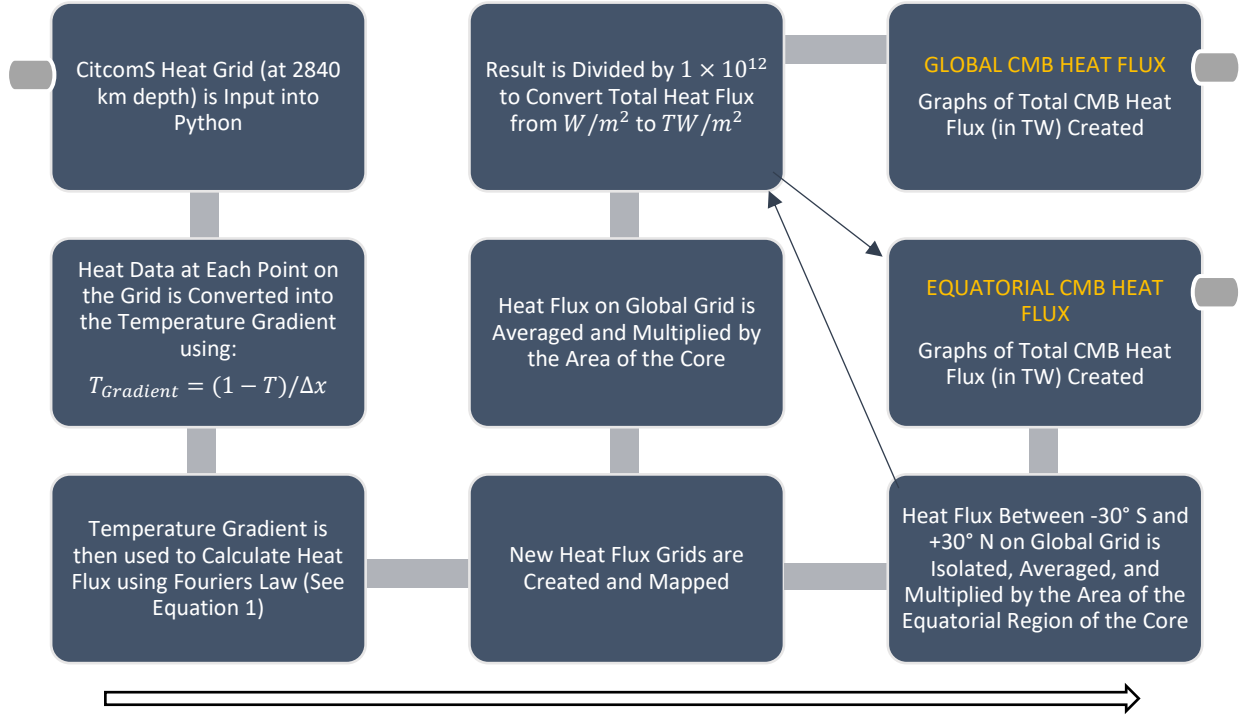
1.5.1 The Equatorial Region and LLSVPs

Isolating the equatorial region of the CMB is important to this project as previous studies have suggested that CMB heat flux variation within this region has the most impact on the geomagnetic reversal rate. In addition to this, the two LLSVPs that reside upon Earth's CMB presently lie within the equatorial regions.

We treat the global and equatorial fields of the CitcomS heat grid outputs separately in analysis, in order to analyse if the equatorial region of the outer-core displays a similar affect upon geomagnetic field reversal rate activity, as shown in previous studies. We define the equatorial region of Earth as the area between -30° S and $+30^\circ$ N and the total area of the Equatorial region of the outer-core was computed as that of a spherical segment between $\pm 30^\circ$ latitude.

1.5.2 Total CMB Heat Flux

In order to calculate total CMB heat flux for each 20 Myr timestep between 1 Ga and present day, the CitcomS heat grids are manipulated as follows:



1.5.3 Core-Mantle Boundary Heat Flux Variability (q^*)

The quantity q^* , also known as the heat flux ratio or amplitude of heat flux heterogeneity, and can be defined as:

$$q^* = \frac{q_{max} - q_{min}}{q_{avg}} \quad (\text{Equ. 3})$$

, where q_{max} , q_{min} , and q_{avg} are the maximum, minimum and average heat flux values at a certain timestep. Choblet, Amit and Husson, (2016) use q^* within their investigation into the coupling of mantle convection, the GPTS and geodynamo simulations. Choblet *et al.* (2016) and Olson and Christensen, (2002) found that q^* is a suitable proxy for the reliability of models, because a high correlation coefficient between q^* and the geomagnetic reversal rate

denotes a successful modelled output of CMB heat flux. Within this project q^* is calculated in the same way, using heat flux data from the predicted CMB heat flow grids, and separated into global and equatorial CMB region tests.

1.5.4 Spherical Harmonics Analysis

Spherical Harmonics are a series of special orthogonal functions that are defined on the surface of a sphere. Spherical harmonic analysis is a natural consequence of Laplace's equation in spherical coordinates, in which harmonic functions satisfy. A harmonic function can be written in terms of sinusoidal and cosinusoidal functions, pertaining to simple harmonic motion of an object. These functions can be expanded onto a unit circle (Fourier analysis), and then from two dimensions to three, onto a unit sphere, creating a set of spherical harmonics. Spherical harmonics analysis is used widely in physics, and commonly undertaken when analysing the geomagnetic field of Earth and other planetary bodies (Harrison, 2006). Based upon discrete numerical data scattered on a spherical surface, spherical harmonics analysis allows for the allocation of a specific function that is applicable to the entirety of the sphere, reflective of the data present. This can be used to extrapolate and interpolate the behaviour of the data to regions with no measurements at all, or to globally 'decompose' the data based upon the wavelength of the signal. We use the latter option here to decompose the CMB heat flux signal into areas of small wavelength (stronger heat flux signal), and large wavelength (weaker heat flux signal). We do this to compare the CMB heat flux signal over time in equatorial regions versus polar regions of Earth.

Spherical harmonics can be sorted into spherical harmonic functions of degree l and order m (Y_l^m), the projection of the functions on a spherical surface are shown in Figure 13 below.

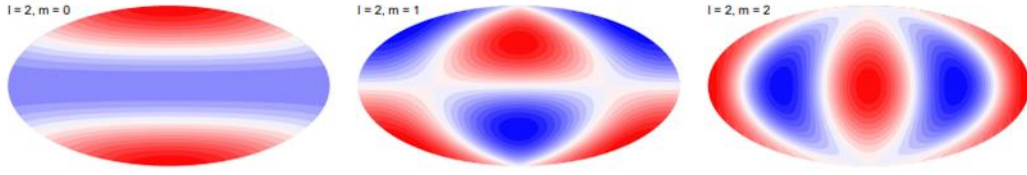


Figure 13) Spherical Harmonic degree and order configurations on a spherical surface for (from left to right) degree two order: zero, one and two. Source: Becker, W. T, 1997 – 2021.

We investigate both Y_2^0 and Y_0^0 . When spherical harmonics are expanded upon a spherical surface the spectra of power of each spherical harmonic degree can be calculated from the decomposed signal. The smaller the spherical harmonic degree (i.e., degree 1, 2, 3), the larger we expect the power (of the signal) the degree encompasses (Fig. 14, 15). In this project we decompose the signal into degrees 1 – 12, this is sufficient as the power contribution from the magnetic field is concentrated within the first ~15 spherical harmonic degrees (Wei-Jia Su *et al*, 1994), as shown in Figure 14.

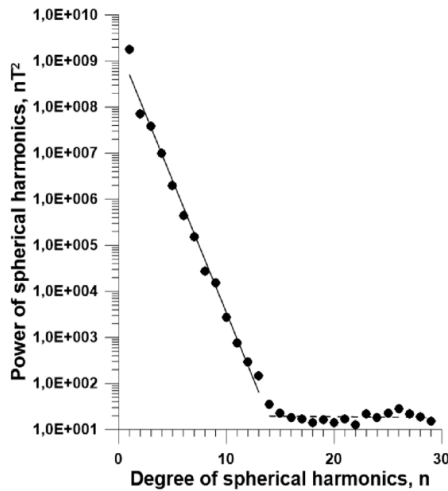


Figure 14) logarithmic power of spherical harmonic degree against the degree itself, for the geomagnetic field. Solid line= power contribution from the core, dotted line= power contribution from the crust. Source: (PT *et al*, 2019)

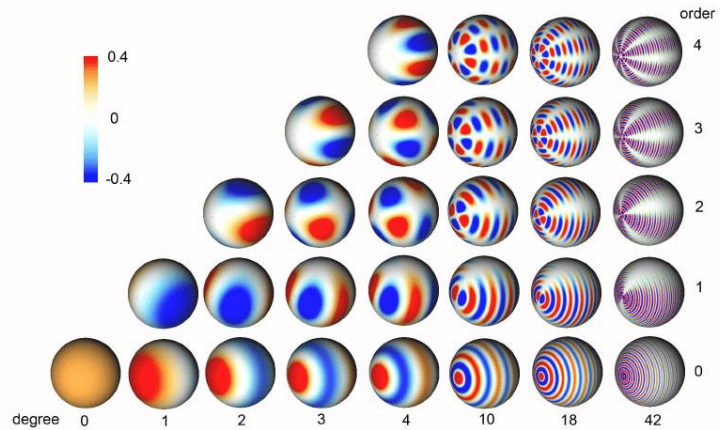


Figure 15) Spherical Harmonic degree and orders on a three-dimensional spherical surface, colour bar representing spherical harmonic degree coefficients. Source: (Chung, Dalton and Davidson, 2008)

Additionally, as seen in Fig. 15, degree 0 order 0 (Y_0^0) encompasses the entire sphere, whereas degree 10 order 4 (Y_{10}^4) defines much smaller regions of the sphere. Y_2^0 is important to consider when investigating equatorial verses polar region CMB heat flux and its

influence on the geomagnetic field because the Y_2^0 structure decomposes the signal into two regions, high latitudes in the north and south, and the low latitudes of the equatorial region of the sphere (Fig. 13) (Amit and Olson, 2015). CMB heat flux signal for each modelled case in 20 Myr increments from 1 Ga to present, is expanded in spherical harmonic degrees 1 – 12 using PySHtools in Python, and the outputs are re-mapped to display the variation in signal dominance between the equatorial and polar regions of Earth (in the Y_2^0 case) and the overall signal strength over time (in the Y_0^0 case). Spherical harmonics of the CMB heat flux data, once extracted, is graphed against time for all models.

1.6 Pearson Correlation

Pearson correlation involves assessing the magnitude and direction of the statistical association or relationship between stationary datasets. The coefficient of Pearson correlation (or Pearson r) produces the normalised measurement of the covariance between two sets of data. Pearson correlation is used within this project to assess the linear relationship between CMB heat flux data results for each modelled case, and the two geomagnetic reversal rates. Pearson r results show whether the two variables considered show a positive, negative, or absence of relationship between the trends of each dataset; where +1 reflects a strong positive relationship, -1 reflects a strong negative relationship, and 0 reflective of no relationship at all (Fig. 16).

Pearson correlation was undergone between Hounslow *et al* (2018) and Olson *et al* (2013) geomagnetic reversal rates, and between CMB heat flux data and both geomagnetic reversal rates. Pearson correlation was undertaken before and after applying a rolling average to both variables used, using pandas and SciPy functions within Python. Rolling average

windows of 60 Myr and 100 Myr were chosen for the data during the correlation process.

This entire process was repeated twice, first for the original CitcomS gridded CMB heat flux data, and then for CitcomS CMB heat flux gridded data with TPW correction applied.

Graphical representation of Pearson r results was created in Excel and edited in Python.

Due to the lack of TPW data beyond 520 Ma, Pearson correlation undergone within this project is limited to this time period. Additionally, to account for the difference between the reversal rates investigated, a separate Pearson correlation analysis was carried out for the last 300 Ma due to the peak in reversal rate activity at ~350 Ma contained in Hounslow *et al* (2018) but not in Olson *et al* (2013).

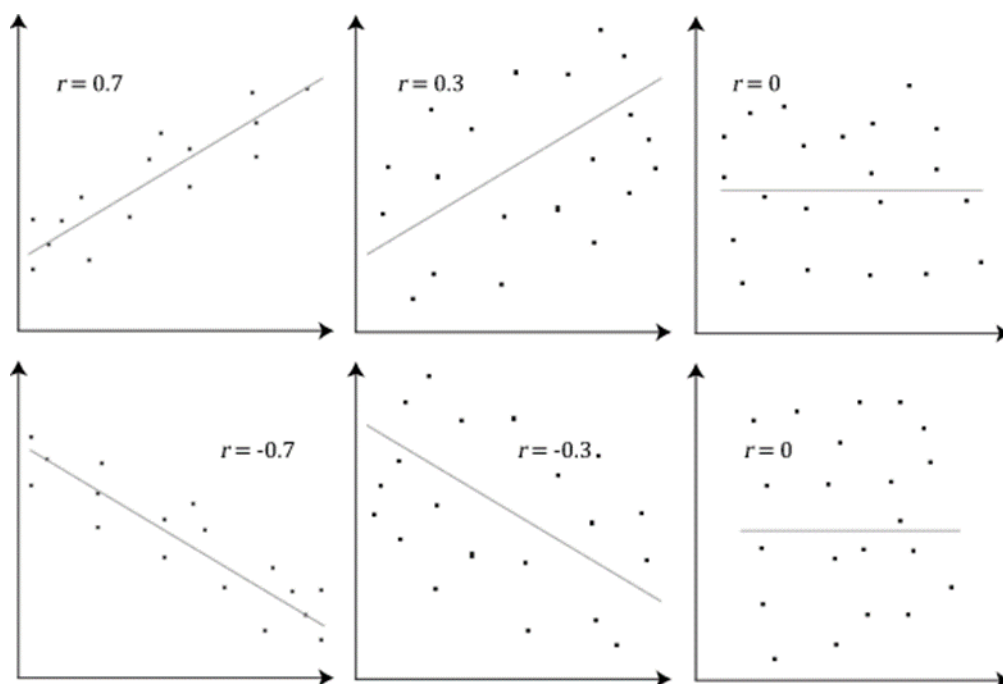


Figure 16) Strength of Pearson's r based upon data relationship. Source: © 2018 Lund Research Ltd, <https://statistics.laerd.com/statistical-guides/img/pc/pearson-2-small.png>

3 Results

CMB heat flux results for each model case (Table 1) were mapped globally in 20 Myr increments, and various quantities were defined and graphed numerically against time and Hounslow *et al* (2018)/ Olson *et al* (2013) reversal rates. This was done to examine the proposed link between CMB heat flux and the geomagnetic field reversal rate.

Results show that there is a weak correlation between superchron occurrence and CMB heat flux magnitude, amplitude, and variability over Earth's history. We see a lack of correlation between total Global and Equatorial CMB heat flux with the geomagnetic reversal rates investigated, which is contradictive of most studies suggesting that total Equatorial CMB heat flux is the most effective in influencing reversal rate behaviour (Glatzmaier *et al.*, 1999; Kutzner and Christensen, 2004; Olson *et al.*, 2010; Olson and Amit, 2014). There is no correlation between global q^* and the reversal rates; However, equatorial q^* and the geomagnetic reversal rates display the strongest overall correlation across all modelled cases, consistent with the concept that equatorial heat flux variation is most likely to influence magnetic field reversals (Nakagawa and Tackley, 2008; Mound *et al.*, 2019). We do, however, see some evidence for a 200 Myr trend in peak-to-trough reversal rate activity when investigating the spherical harmonic degree 2 order 0 of the CMB heat flux fields.

In regard to the variations in modelled cases investigated, final graphical results of defined quantities, as well as mapped spatial distribution of CMB heat flux, both reflect the impact of changing the initial basal layer density and tectonic reconstruction corrections of each modelled case respectively.

3.1 Evolution of CMB Heat Flux Through Time

3.1.1 Spatial Representation of CMB Heat Flux

CMB heat flux evolution over time for each modelled case was closely dependent on the initial basal layer density and rotations applied to the models (Fig. 17,18,19). Total global CMB heat flux is seen to slowly increase over time toward present day for all modelled cases. Case 1 which is purely thermal, displays a very high signature of CMB heat flux through time (Fig. 17). Considering that in this case, the basal layer density is the same as the ambient mantle, the basal layer is freely moved and circulated through the mantle over time, which in turn created a relatively large temperature gradient between the lower mantle and the CMB, causing a higher flux of heat from the CMB into the lower mantle.

Case 2 displays distinctively low CMB heat flux beneath Africa and the Pacific. This is representative of the two LLSVP's present on earth today (Tuzo and Jason, Fig. 7) which display movement over time throughout all model cases. These structures display a low CMB heat flux signature beneath them because they are hotter and chemically distinct from the surrounding mantle. The hot LLSVPs create a distinctively small temperature gradient between the CMB and the base of the structures, acting as an insulator of heat at the CMB and thus suppressing CMB heat flux to the mantle. The basal layer density of Case 2 was +1% larger than the surrounding mantle material, thus, the basal layer was able to remain within the deep mantle and prevent itself from being circulated through the mantle and dampening its insulative effect on the CMB, as seen with case 1 (Fig. 17).

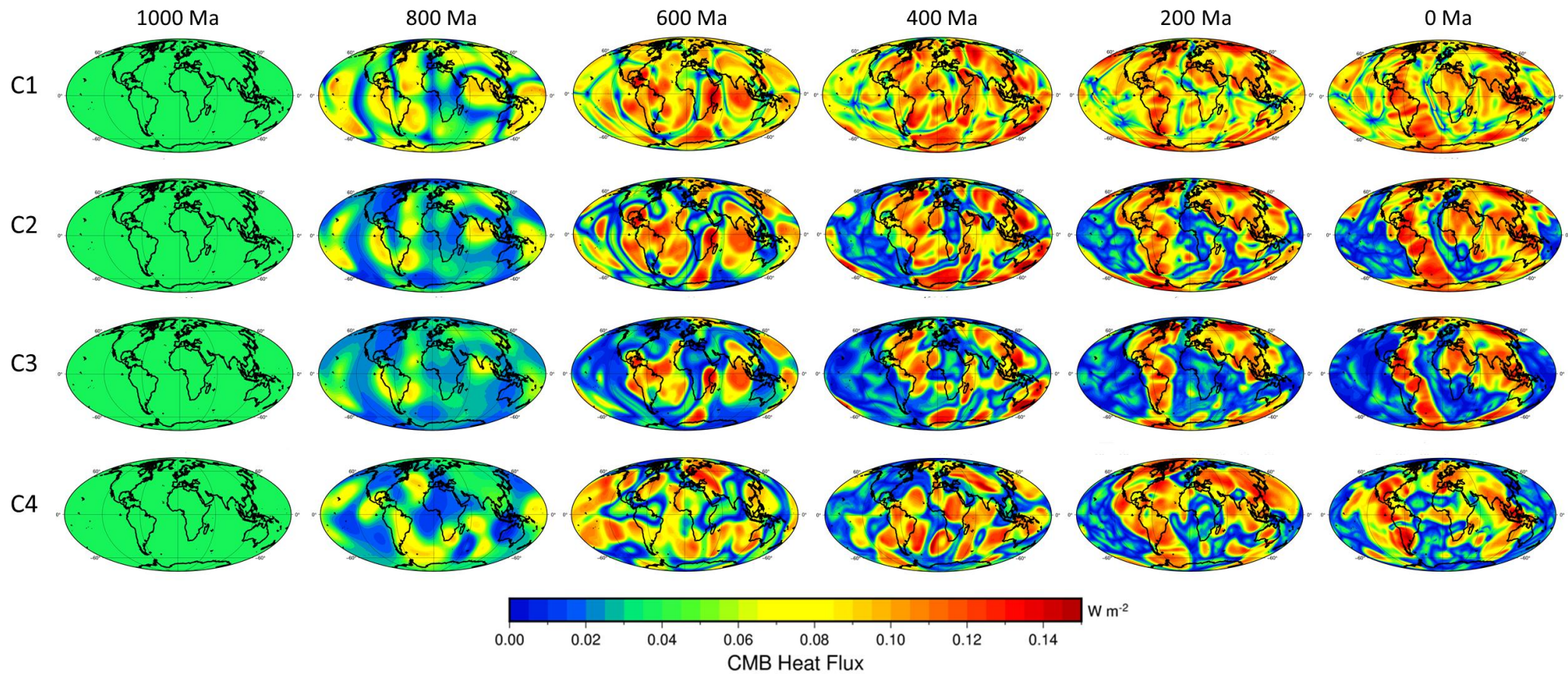


Figure 17) Spatial distribution of CMB heat flux for all model cases in 200 Myr increments. Results above are CMB heat flux data without TPW correction applied. Colour bar denoting low CMB heat flux blues/greens, and high CMB heat flux orange/reds. Present-day coastlines are outlined in black. Global maps created in Python.

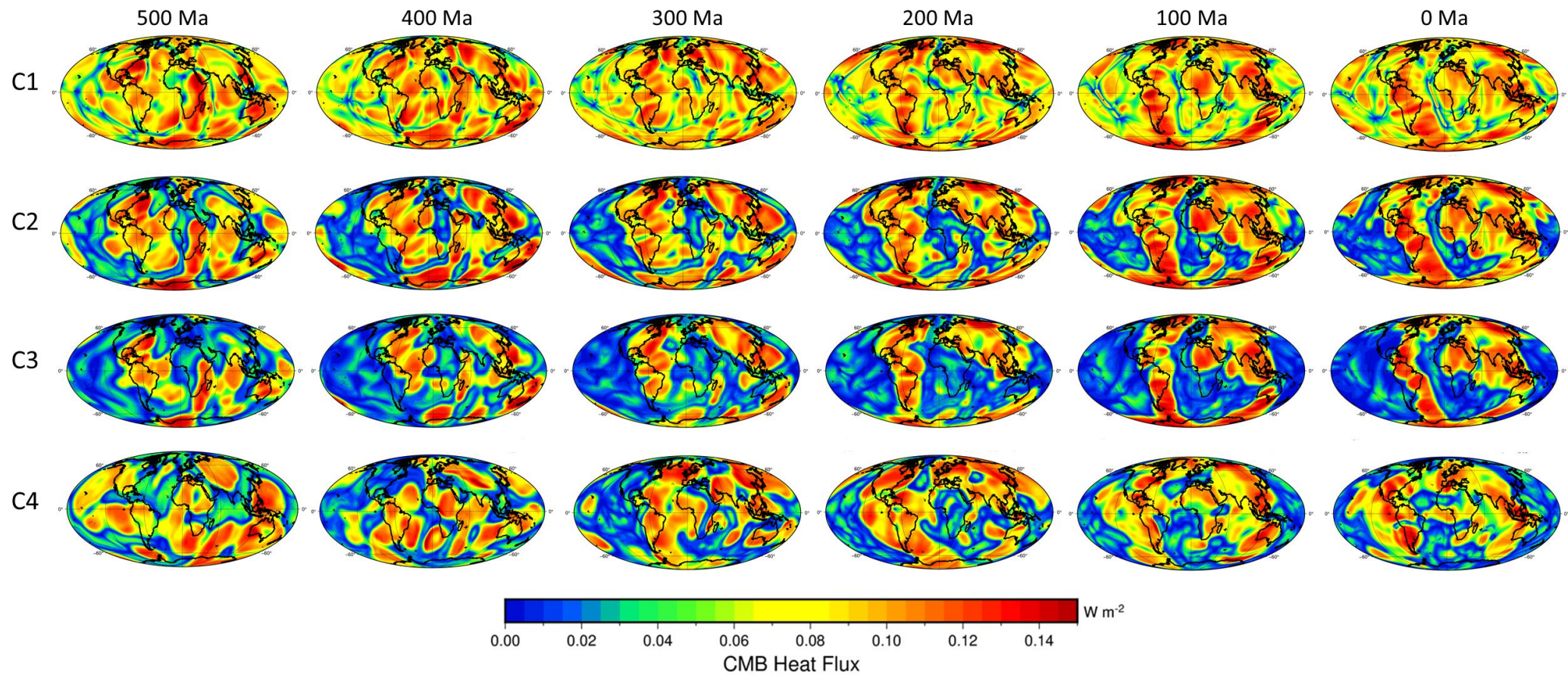


Figure 18) Spatial distribution of CMB heat flux for all model cases in 100 Myr increments. Results above are CMB heat flux data without TPW correction applied. Colour bar denoting low CMB heat flux blues/greens, and high CMB heat flux orange/reds. Present-day coastlines are outlined in black. Global maps created in Python.

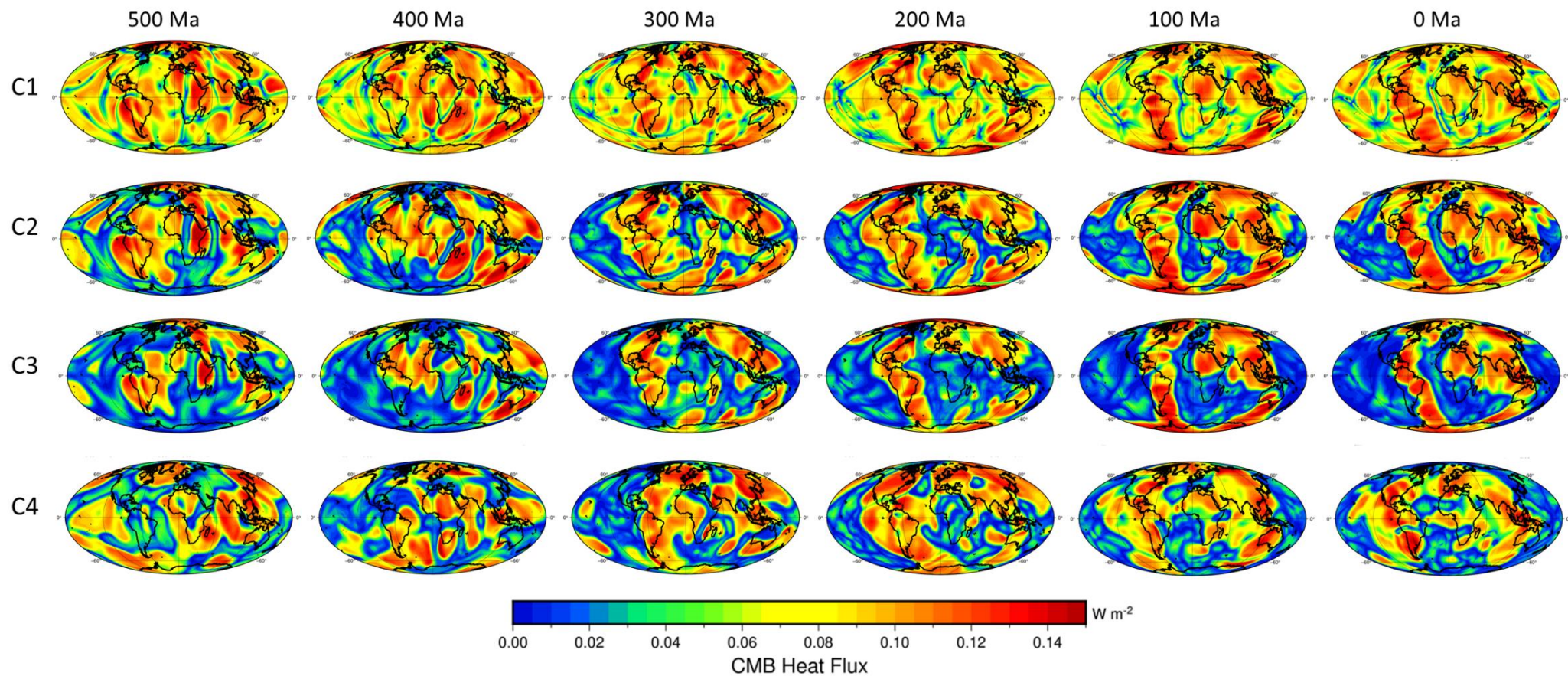


Figure 19) Spatial distribution of CMB heat flux for all model cases in 100 Myr increments. Results above are CMB heat flux data with TPW correction applied. Colour bar denoting low CMB heat flux blues/greens, and high CMB heat flux orange/reds. Present-day coastlines are outlined in black. Global maps created in Python.

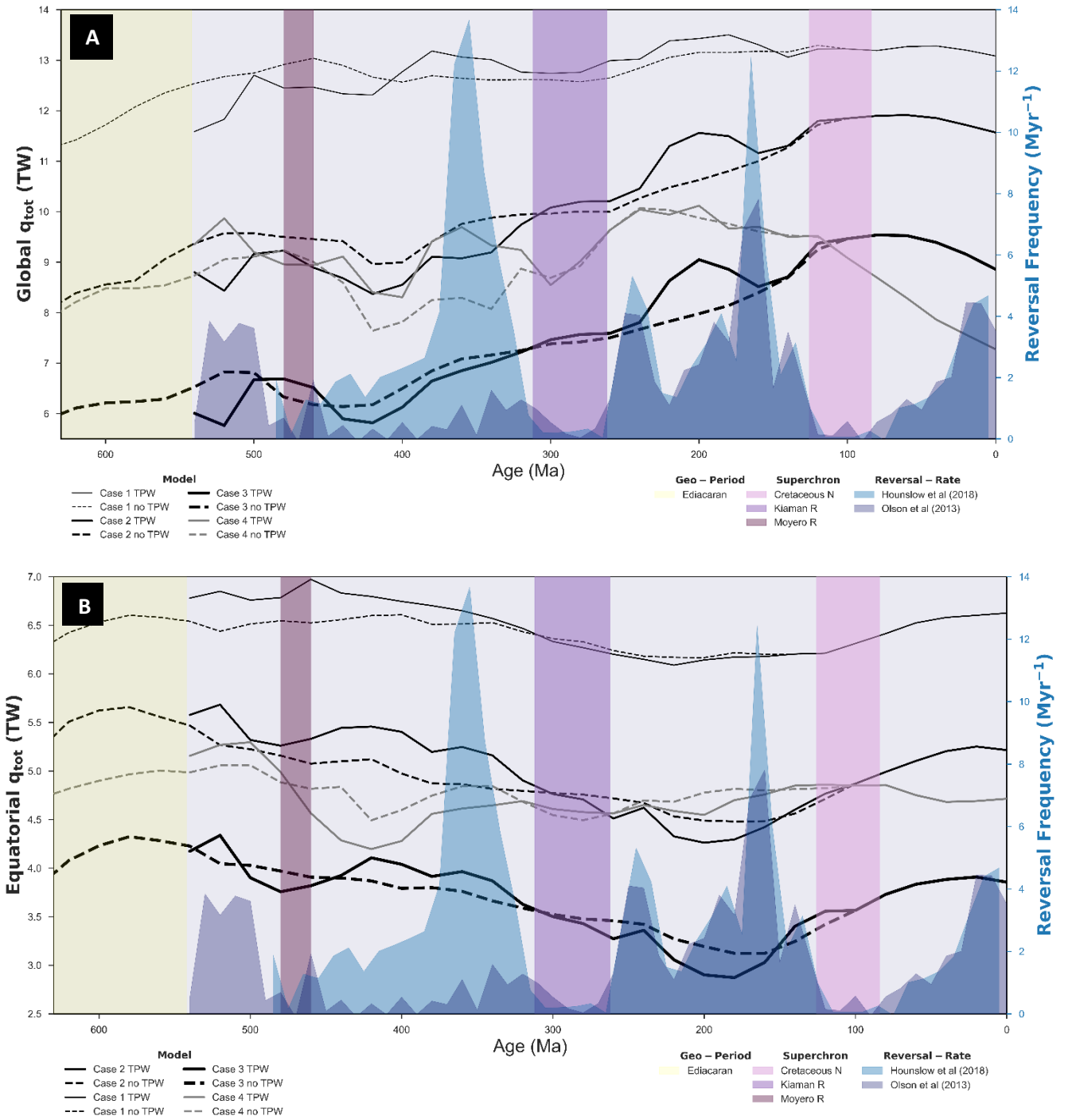
Case 3 contains the densest basal layer, +2% greater than the surrounding mantle; The evolution of the mantle flow model shows that alteration of the basal layer in this way created a similar effect upon CMB heat flux to that of Case 2, however areas in which CMB heat flux is suppressed, is greater and more widespread in areas in which LLSVP structures reside.

Case 4 has the same basal layer density as Case 2; however, it is the only modelled case without net rotation removed. The difference in spatial distribution of CMB heat flux in Case 4, contrasts greatly with the previous cases without net rotation. Case 4 at present day does not reflect the current present-day basal mantle structure of Earth that is inferred from tomography. This indicates that net rotation of the lithosphere does not influence basal mantle structure and spatial distribution of CMB heat flux, which is expected (Rudolph and Zhong 2014).

3.1.2 Numerical Representation of CMB Heat Flux

Total CMB Heat Flux for both global and equatorial fields is graphed against time for both the TPW-corrected and no-net rotation reference frames. Total global CMB heat flux shows a gradual increase over time from ~600 Ma to present (Fig. 20 A), whereas total equatorial CMB heat flux displays a gradual decline over time (with exception of case 4) until ~200 Ma, followed by a gentle increase to present-day (Fig. 20 B). Neither quantity reflect trends in the geomagnetic reversal rates from both studies. All cases seem to remain consistent in trend over time with exception to case 4, attributable to its different reference frame. Application of TPW correction shows a change in magnitude of CMB heat flux across both quantities, the

most striking change seen within Fig. 20 A, where bulging occurs at ~200 Ma with TPW correction applied, compared to a relatively gradual incline when TPW is not considered.



3.1.3 Spherical Harmonics of CMB Heat Flux

I analyse the evolution of Y_0^0 and Y_2^0 coefficients for all models. At ~600 Ma, the overall signal from the outputs declines at a rapid rate until the 1000 Ma limit is reached (Fig. 21). This trend in signal strength is attributed to model ‘start-up’ where time is taken for tectonic movement on the surface of the shell to start and initiate subduction of slabs into the mantle, which helps drive convection in the mantle and induces variability in heat in the deep earth. This suggests that the models were not in dynamic equilibrium before 600 Ma (during the period before the slabs reached the mantle) and cannot be analysed before this point.

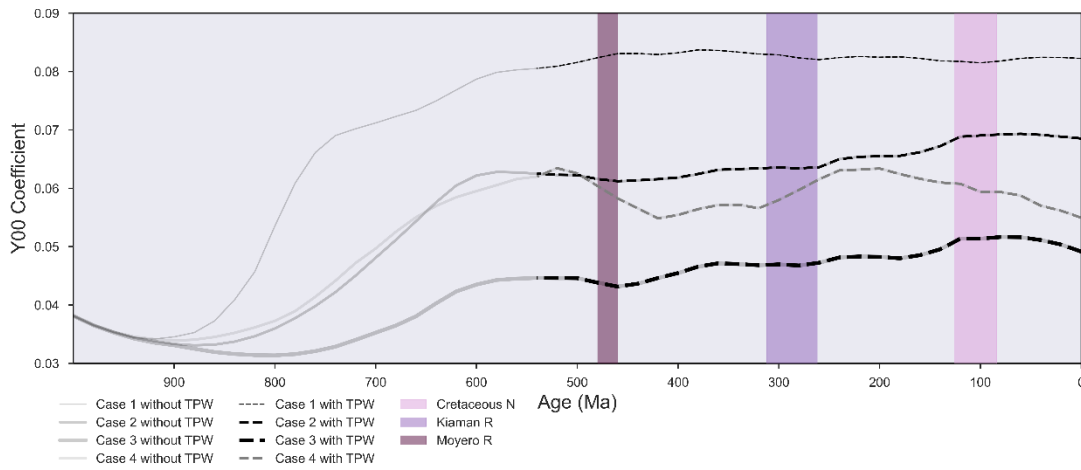
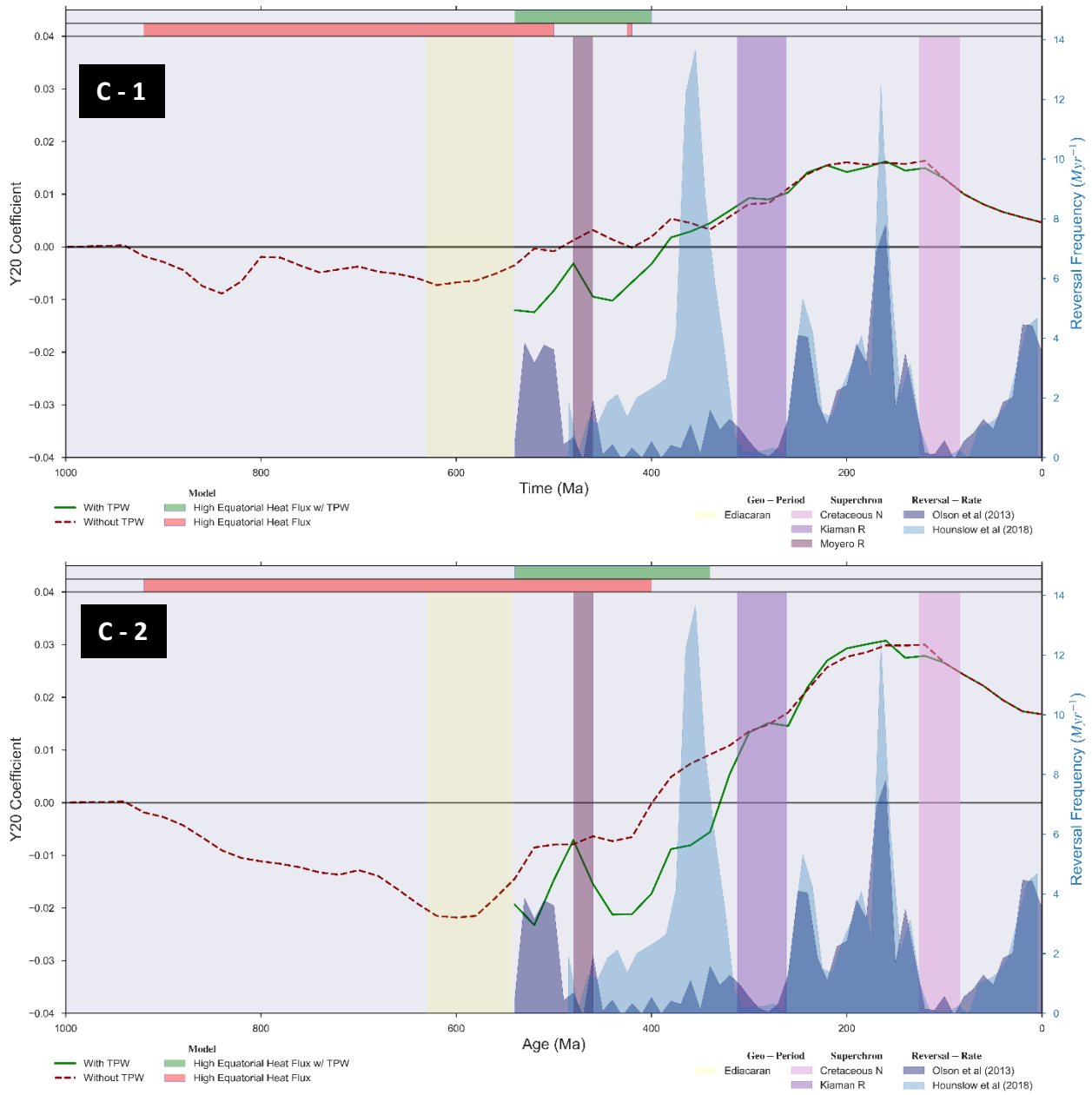


Figure 21) Y_{00} structure against time for all model cases. Thickness of data lines corresponding to basal layer density imposed upon mantle flow simulation in CitcomS, in which data is derived. Case 4 is in grey compared to black to differentiate between case 2 and case 4 in basal layer density, as it is the same for both cases.

Degree 2 order zero structure of the CMB heat flux signals (Y_2^0) for all modelled cases all distinctively display a large bell curve trend, with a 200 Myr peak-trough cycle. The peak in Y_2^0 at ~180 Ma coincides with a period of high reversal frequency, captured in both geomagnetic reversal rates considered. The second high reversal frequency peak at ~370 Ma defined by the Hounslow et al (2018) reversal rate, however, does not follow the same trend with the degree 2 data, instead, there is a great decline during this period. Y_2^0 displays relatively low intensity in some cases before both Kiaman and Moyero superchrons, with the

Cretaceous Normal Superchron being the exception, in which the power only rapidly decreases once the superchron period had commenced (Fig. 22).

In model cases 1,2 and 3, TPW corrected Y_2^0 all display a slow increase and rapid decrease in power when progressing through the Ediacaran period. Y_2^0 peaks at the beginning of the Ediacaran period and progressively decreases through the event.



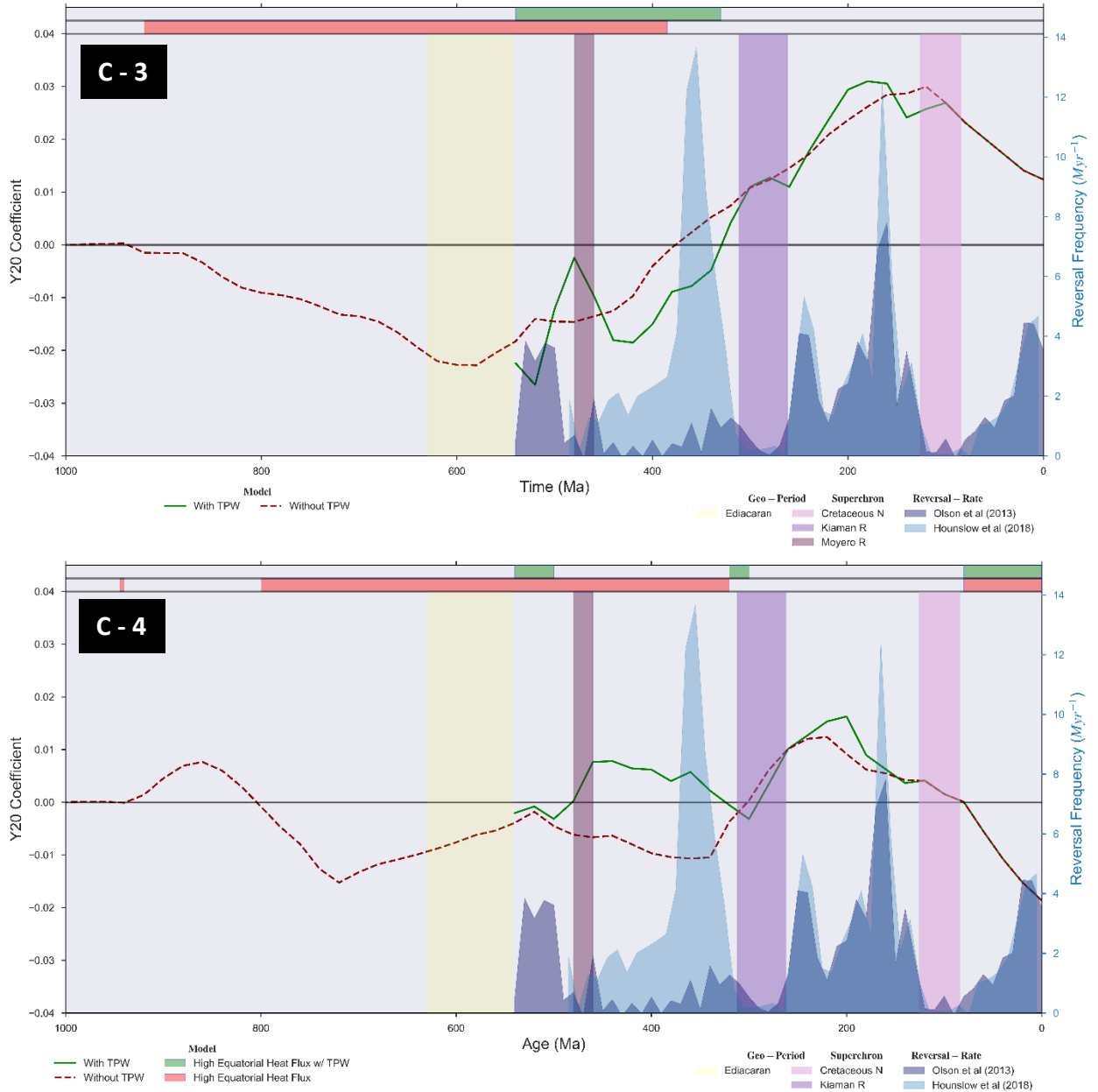


Figure 22) (a) 'Flip' in CMB heat flux signal dominance from polar regions to equatorial regions between 380 – 420 Ma (See Appendix A for more details) under the expanded spherical harmonic degree two order zero structure. Y_2^0 coefficient for all modelled cases with and without TPW correction, over time. C - (x) refer to the modelled cases C1 – 4.

3.2 Evolution of q^* Over Time

In most modelled cases, global q^* displays an overall increase (Fig. 23), whereas equatorial q^* displays an overall decrease when moving forward in time. Cases 1,2 and 3 all show an increase in q^* global during the high reversal rate frequency period between ~160 – 240 Ma.

Equatorial q^* for cases 1 and 2 is seen to slightly increase or remain relatively constant during all superchron periods, where global q^* seems to follow no trend throughout these periods.

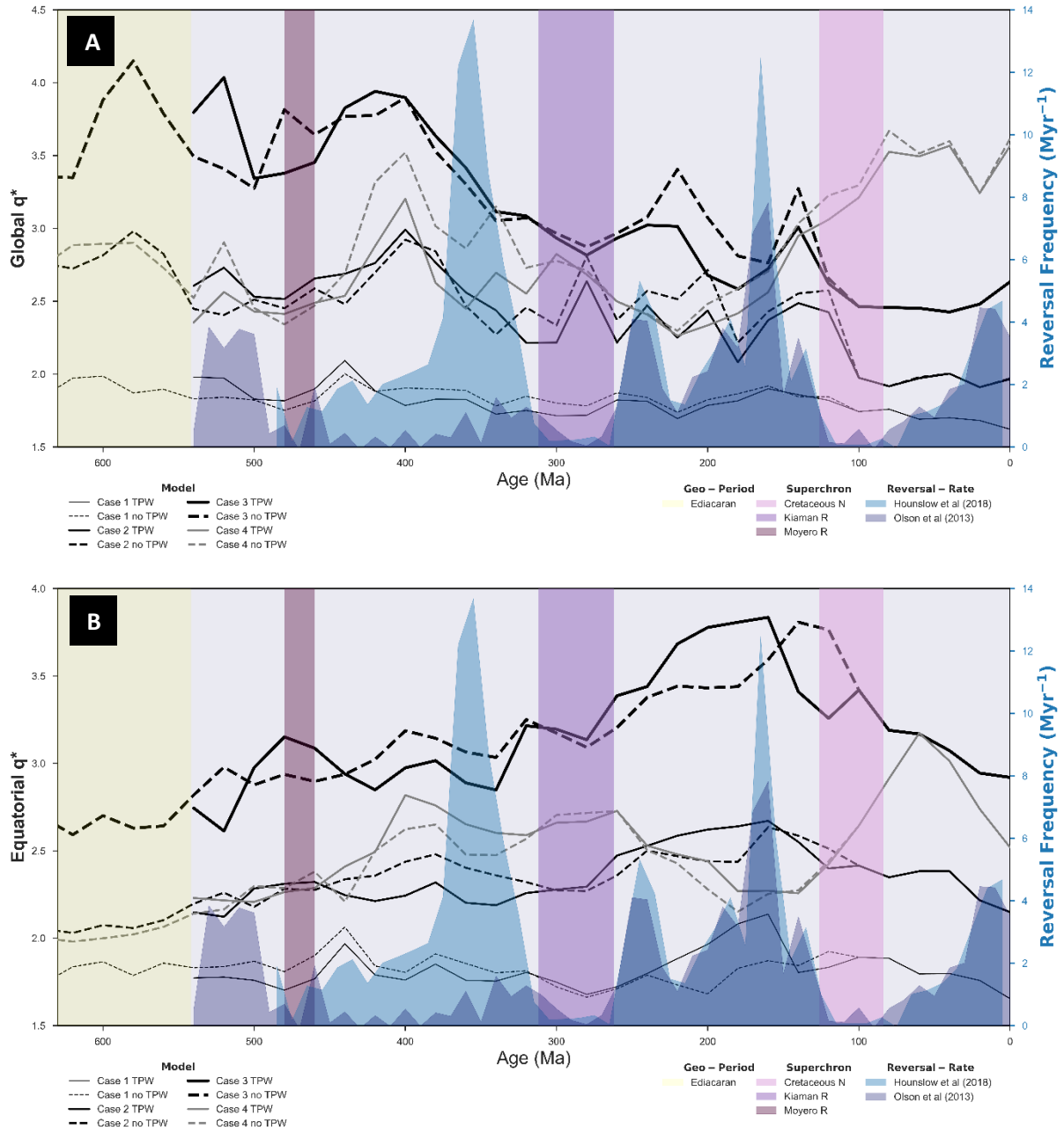


Figure 23) Global (A) and equatorial (B) q^* for all modelled cases over time with and without TPW correction. Thickness of data lines correspond to basal layer density imposed upon mantle flow simulation in CitcomS, in which data is derived. Case 4 is in grey compared to black to differentiate between case 2 and case 4 in basal layer density, as it is the same for both cases.

3.3 Pearson Correlation of Results

Pearson correlation was computed in 10 Myr increments for total q and q^* for both global and equatorial fields of each modelled case against both Hounslow *et al* (2018) and Olson *et al* (2013) geomagnetic reversal rates. This correlation includes the CMB heat flux fields with and without TPW correction applied and with and without a rolling average (60 Ma and 100 Ma windows) applied to the data. Pearson correlation here is limited to 520 Ma for which TPW-correction is available.

Pearson correlation between the two reversal rates over a 520 Myr period peak at 0.43 when under a 100 Myr rolling window. It can be assumed that this Pearson r is low because of the lack of high reversal period at ~350 Ma within the Olson *et al* (2013) reversal rate (Fig. 22).

When we limit the correlation test to 300 Ma however, the correlation between both reversal rates peak at 0.78.

Equatorial q^* has an average of 0.35 r when restricted to 520 Ma and 0.47 r when restricted to 300 Ma, when correlated against the Olson *et al* (2013) reversal rate. After restricting analysis to 300 Ma, Equatorial q^* before averaging, and with TPW correction applied, has the highest Pearson r when correlated against both reversal rates. In addition, all other tests designed for Pearson correlation analysis display a positive correlation between equatorial q^* and both reversal rates under the conditions of Case 2.

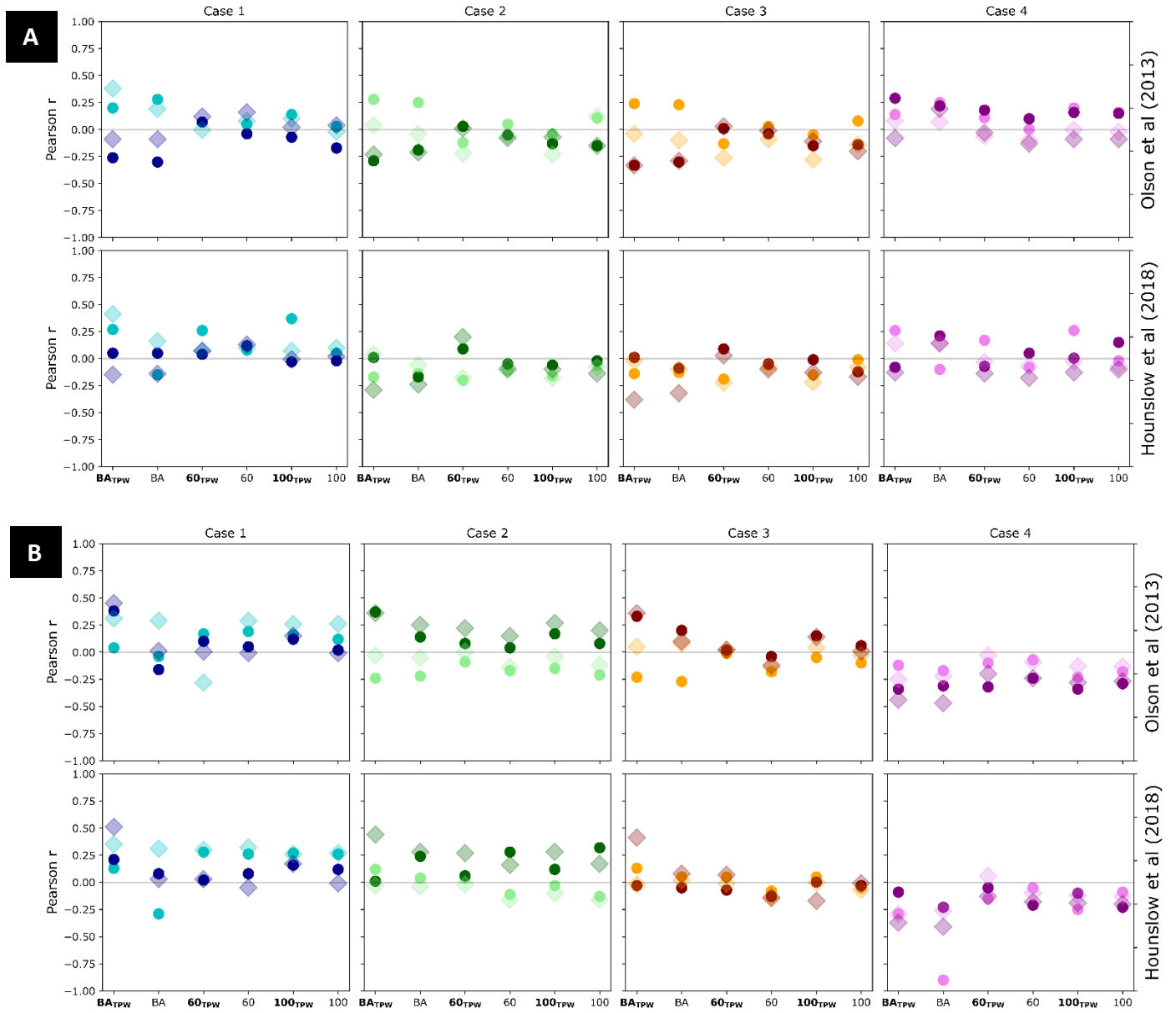


Figure 24) Pearson correlation between CMB heat flux data and Hounslow et al, (2018), Olson et al (2013) reversal rates. Three main Pearson correlation tests of CMB heat flux data: Before Averaging (BA), After averaging with a 60 Myr and 100 Myr window (60) and (100) respectively, as well as their TPW-corrected counterpart. Lighter colours correspond to global field data, and darker counterparts that of equatorial field data. Circular markers represent Pearson correlation tests with a limit of 520 Ma, and diamonds that of 300 Ma. (A) Pearson correlation of q total data with reversal rates. (B) Pearson correlation of q^* data with reversal rates.

4 Discussion

4.1 Impact of Initial Model Conditions on CMB Heat Flux

4.1.1 Application of True Polar Wander

TPW and its importance regarding the movement of the geomagnetic poles over Earth's history, is apparent within this study. After applying TPW correction to CMB heat flux data, Pearson correlation between CMB heat flux data and both Hounslow et al (2018) and Olson et al (2013) reversal rates almost always display a higher Pearson r compared to that of data without TPW applied (Fig 24). The application of TPW correction also reveals sharp bell curves in Y_2^0 and global total q in all modelled cases that coincide with high reversal rate activity more-so than CMB heat flux without TPW applied. This result supports the argument that connects TPW with magnetic field hyperactivity, implying that TPW movement is a surface response to core/deep mantle/geodynamo evolution and the stability of the magnetic field (Biggin *et al.*, 2012; Meert *et al.*, 2016). TPW further back in time is not constrained and data are scarce, thus many limitations of TPW are apparent in this study in regard to the validity of TPW correction moving further back in time.

4.1.2 Basal Layer Density

Variation in basal layer density between each modelled case resulted in large variations not only in spatial representation of CMB heat flux (Fig. 17,18,19), but also in CMB heat flux magnitude, amplitude (Fig. 17 – 21) and rate of change over time (Fig. 23). Case 2 (Table 1), reflects CMB heat flux spatial pattern reminiscent of LLSVP structure (Fig. 17, 18, 19) (Flament *et al.*, 2017; Niu, 2018); whereas cases with lower (Case 1) and higher (Case 3) basal layer densities (Table 1) display exponentially higher and lower CMB heat flux signals

respectively. This effect is present in both the spatial and numerical results of CMB heat flux over time. The relative trending of all CMB heat flux results for Cases 1 and 3 compared to that of Case 2, were not altered sufficiently; instead, the overall magnitude of the quantities was changed, with case 1 positioned higher in CMB heat flux signal magnitude, Case 2 remaining in the middle, and case 3 within the lowest magnitude. Figures 17 19 and 20 display this change clearly. This result is in agreement with the argument that the basal layer and its LLSVP structures are denser than the surrounding mantle and exhibit the ability to insulate the CMB, by decreasing the temperature gradient and suppress CMB heat flux (Li, Zhong and Olson, 2018).

4.1.3 Net Rotation of the Lithosphere

The idea that Net Rotation of the lithosphere does not impact the geodynamo and its behaviour, is clear within this study. Case 4, containing the same basal layer density as case 2 (Table 1), but unlike the other three Cases, does not have Net Rotation removed from its tectonic reconstruction used within CitcomS mantle flow simulation. The inclusion of Net Rotation in this case, caused this model to behave differently in simulation and hence produce completely contrasting CMB heat flux results compared to the first three cases. In all results above, it is apparent that the trend in CMB heat flux amplitude, spread, magnitude, and rate of change, all barely follow the general trend of the other cases. Case 4 CMB heat flux data follows no trend similar to that of reversal rate activity and displays the most negative Pearson r across all quantities within Pearson Correlation analysis (Fig. 24).

4.2 CMB Heat Flux and the Geomagnetic Field Reversal Rate

Results infer that global CMB heat flux over Earth's history has been increasing slowly toward present day. Global CMB heat flux itself displays no direct correlation to the geomagnetic reversal rates investigated, without TPW applied. When TPW is applied to global total q some bulging occurs in areas where high reversal rate activity prevails (Fig. 20 A) and Pearson r for this quantity is higher. However, this is not consistent for all modelled cases. This is to be expected, as previous studies show that the polar contribution to global total q does not impact geodynamo function nor the intensity of the magnetic field (Olson *et al.*, 2010).

Total equatorial q results (Fig. 20 B) contrast the findings of previous studies, suggesting that the geomagnetic field and its intensity/reversal frequency is most sensitive to change in total equatorial q (Glatzmaier *et al.*, 1999; Kutzner and Christensen, 2004). We find that total equatorial q is weakly correlated (Fig. 24 A) to the reversal rates than that of total global q which is unexpected. Reasons as to why this may have occurred may be linked to numerical limitations that arise in regard to model accuracy and mantle flow simulation, including such computational limits, such as viscosity contrasts and Ra as previously mentioned.

4.3 Q^* and the Geomagnetic Field Reversal Rate

Global and equatorial q^* for all modelled cases display trends inverse of total global and equatorial q discussed above. The order in which previous cases followed in terms of magnitude is now reversed, as q^* reflects the variability/heterogeneity of CMB heat flux. As expected, Case 1 remains in lower magnitudes of q^* as heat distribution at the CMB is homogenous (Fig. 17) and thus, the heterogeneity of CMB heat flux is small. As we progress

through the other modelled cases, basal layer density increases, and homogeneity decreases with the establishment of the basal layer structures upon the CMB, causing the successive increase in q^* respectively for each case. This is again consistent with the behaviour and nature of the LLSVP structures and that previous studies suggest (Li, Zhong and Olson, 2018).

Global q^* displayed a very low Pearson r across all modelled cases and resulted in the worst performing quantity. Global q^* is stochastic and ignores all trend in reversal frequency over time. This result is similar to that of Choblet, Amit and Husson (2021), in which only one model within their investigation satisfied the requirements to suggest global q^* is viable.

Equatorial q^* however, is the strongest of all quantities investigated in terms of correlation and trend with both reversal rates. Equatorial q^* relates much closer to the trend of reversal frequency of the magnetic field, with all modelled cases except for case 4, peaking during high reversal rate activity between the end of the Kiaman reverse to the start of the Cretaceous normal superchron. Additionally, equatorial q^* does not acknowledge the second period of high reversal rate activity between the Moyero and Kiaman reversed superchrons.

4.4 The Ediacaran Period and 200 Myr Cycle

The Ediacaran period, the EEE and the hypothesised 200 Myr cycle in reversal frequency is best observed within the spherical harmonic analysis results of this project.

Y_2^0 of the CMB heat flux signals for each modelled case (Fig. 22) display a distinct bell curve correlating with the high reversal frequency period between the Kiaman reversed and Cretaceous normal superchrons. Across all models, Y_2^0 dips to its lowest point right before

both Moyero and Kiaman superchron periods coinciding with the proposed Mid-Palaeozoic dipole low between 460 – 322 Ma of Hawkins et al (2021). Hawkins et al (2021) also proposes a substantial increase in field strength before the onset of the Cretaceous normal superchron, which is also seen here within Y_2^0 of the CMB heat flux data for modelled Cases 1, 2 and 3. In addition to this, Y_2^0 also displays one successful 200 Myr peak-to-trough cycle from 400 Myr to present day. The cycle is interrupted by a sharp decrease in Y_2^0 right at the beginning of the Moyero superchron when considering the TPW corrected dataset, however, the dataset without TPW applied continues into the Ediacaran period and all modelled cases display a sharp decline in coefficient, signifying that the equatorial region of the simulations at this time dominated in CMB heat flux magnitude and as a result, could have contributed to a period of high reversal frequency of the magnetic field. This result supports evidence to suggest that a period of high geomagnetic reversal frequency occurred during the Ediacaran Period, weakening the dipole of the field and contributing to the oxygen loss within the atmosphere and UV radiation exposure of the land surface during this time, contributing to the EEE extinction event at the end of the Ediacaran (Wei *et al.*, 2014; Lee *et al.*, 2016; Meert *et al.*, 2016; Bono *et al.*, 2019; Hawkins *et al.*, 2021; Thallner, Biggin and Halls, 2021).

4.5 Limitations

Global-scale mantle modelling has evolved rapidly over the 21st century, however, computational limitations still remain in many facets of modelling. Within this study Y_0^0 structure of all modelled cases shows a rapid decrease right after ~600 Ma, this is a consequence of mantle modelling set-up, in which the evolution of the simulation takes time to establish. This cost of time means that the further back in time we analyse, the more pre-mature the simulation is and the less accurate the resultant data produced will be. This is

taken into consideration, as well as the limitations in data availability and consistency considered here, such as TPW correction and both reversal rates used. Temporal resolution of CitcomS CMB heat flux data is a relatively large 20 Myr increments, however, processes that govern magnetic field behaviour and variability over time operate on very large time scales. The interpolation and up-sampling of CMB heat flux data for Pearson correlation analysis was needed to fit the temporal resolution of the reversal rate data (10 Ma) which arises limitation in the accuracy of up sampling data in use for comparison.

The verification and validation of numerical modelling itself is considered a tough feat given the limits and boundaries of current numerical simulation power. Models fall short in replicating viscosity contrasts, Ra contrast, open system interactions and in accurate boundary conditions. The most impactful limitations in the case of modelling the deep Earth is the inability to observe and measure conditions and properties directly (Oreskes, Shrader-Frechette and Belitz, 1994; Steinberger and Calderwood, 2006).

5 Conclusion

The aim of this project was to assess the behaviour of the geomagnetic field from 1 Ga to present day using CMB heat flux as a proxy for the evolution of the geodynamo and hence magnetic field of Earth. We define and investigate various quantities of CMB heat flux such as total q and q^* within both global and equatorial fields, as well as spherical harmonic degree 2 order 0 (Y_2^0), and spherical harmonic degree 0 order 0 structure (Y_0^0). We compare the defined quantities with paleo-geomagnetic reversal rates from two studies and perform various Pearson correlation tests to assess the validity of similar trends between datasets. Our hypothesis dictating that equatorial q would be the deciding factor in influencing

geodynamo behaviour did not agree with results, instead we find that equatorial q^* remains correlated the strongest with the geomagnetic reversal rates over time, although the strongest Pearson r recorded was 0.5. In addition, we find that spherical harmonic degree 2 order 0 (Y_2^0) and q^* global for model cases 1, 2 and 3 all display evidence for an active reversal period during the Ediacaran. Additionally, Y_2^0 displays one successful 200 Myr cycle from 400 Ma to present day. In this project we are limited to 520 Myr when analysing TPW correction and modelled Y_0^0 structure reveals that model accuracy plummets at ~ 600 Myr due to lack of dynamic equilibrium within the model simulation at this time. Findings suggest that equatorial q^* and spherical harmonic degree two order zero structure (Y_2^0), may be useful avenues to investigate when assessing magnetic field intensity and its variability over time, as well as the avenue of linking long-term magnetic field behaviour with Earth's deep mantle cycles.

6 References

(1963), I. & P. (1963) 'The Geophysical', 8(3).

Amit, H. and Olson, P. (2015) 'Lower mantle superplume growth excites geomagnetic reversals', *Earth and Planetary Science Letters*, 414, pp. 68–76. doi: 10.1016/j.epsl.2015.01.013.

Biggin, A. J. *et al.* (2012) 'Possible links between long-term geomagnetic variations and whole-mantle convection processes', *Nature Geoscience*, 5(8), pp. 526–533. doi: 10.1038/ngeo1521.

Bono, R. K. *et al.* (2019) 'Young inner core inferred from Ediacaran ultra-low geomagnetic field intensity', *Nature Geoscience*, 12(2), pp. 143–147. doi: 10.1038/s41561-018-0288-0.

Carbone, V. *et al.* (2020) 'A model for the geomagnetic field reversal rate and constraints on the heat flux variations at the core-mantle boundary', *Scientific Reports*, 10(1), pp. 1–9. doi: 10.1038/s41598-020-69916-w.

Choblet, G., Amit, H. and Husson, L. (2016) 'Constraining mantle convection models with palaeomagnetic reversals record and numerical dynamos', *Geophysical Journal International*, 207(2), pp. 1165–1184. doi: 10.1093/gji/ggw328.

Chung, M. K., Dalton, K. M. and Davidson, R. J. (2008) 'Tensor-based cortical surface morphometry via weighted spherical harmonic representation', *IEEE Transactions on Medical Imaging*, 27(8), pp. 1143–1151. doi: 10.1109/TMI.2008.918338.

Courtillot, V. and Le Mouél, J. L. (2007) 'The study of Earth's magnetism (1269-1950): A foundation by Peregrinus and subsequent development of geomagnetism and paleomagnetism', *Reviews of Geophysics*, 45(3), pp. 1–31. doi: 10.1029/2006RG000198.

- Driscoll, P. and Olson, P. (2009) 'Polarity reversals in geodynamo models with core evolution', *Earth and Planetary Science Letters*, 282(1–4), pp. 24–33. doi: 10.1016/j.epsl.2009.02.017.
- Evans, D. (2002) 'True polar wander and supercontinents', *Tectonophysics*, 362, pp. 303–320. doi: 10.1016/s0040-1951(02)00642-x.
- Flament, N. *et al.* (2017) 'Origin and evolution of the deep thermochemical structure beneath Eurasia', *Nature Communications*, 8(May 2016). doi: 10.1038/ncomms14164.
- Garnero, E. J., McNamara, A. K. and Shim, S. H. (2016) 'Continent-sized anomalous zones with low seismic velocity at the base of Earth's mantle', *Nature Geoscience*, 9(7), pp. 481–489. doi: 10.1038/ngeo2733.
- 'Geochemistry, Geophysics, Geosystems' (2014), pp. 1–13. doi: 10.1002/2014GC005457.Received.
- Glatzmaier, G. A. *et al.* (1999) 'The role of the Earth's mantle in controlling the frequency of geomagnetic reversals', *Nature*, 401(6756), pp. 885–890. doi: 10.1038/44776.
- Gubbins, D., Jones, A. L. and Finlay, C. C. (2006) 'Fall in Earth's Magnetic Field Is Erratic', *Science*, 312(5775), pp. 900 LP – 902. doi: 10.1126/science.1124855.
- Harrison, C. G. A. (2006) 'Variation of spherical harmonic power as a function of harmonic order for Earth's core and crustal magnetic field and for Mars' crustal field', *Geochemistry, Geophysics, Geosystems*, 7(10), pp. 1–17. doi: 10.1029/2006GC001334.
- Hawkins, L. M. A. *et al.* (2021) 'Intensity of the Earth's magnetic field: Evidence for a Mid-Paleozoic dipole low', *Proceedings of the National Academy of Sciences of the United States of*

America, 118(34). doi: 10.1073/pnas.2017342118.

Hounslow, M. W., Domeier, M. and Biggin, A. J. (2018) 'Subduction flux modulates the geomagnetic polarity reversal rate', *Tectonophysics*, 742–743(May), pp. 34–49. doi: 10.1016/j.tecto.2018.05.018.

Irving, E. and Pullaiah, G. (1976) 'Reversals of the geomagnetic field, magnetostratigraphy, and relative magnitude of paleosecular variation in the phanerozoic', *Earth Science Reviews*, 12(1), pp. 35–64. doi: 10.1016/0012-8252(76)90053-2.

Kutzner, C. and Christensen, U. R. (2004) 'Simulated geomagnetic reversals and preferred virtual geomagnetic pole paths', *Geophysical Journal International*, 157(3), pp. 1105–1118. doi: 10.1111/j.1365-246X.2004.02309.x.

Leconte, J. (2018) 'Continuous reorientation of synchronous terrestrial planets due to mantle convection /704/445/862 /704/445/210 /129 article', *Nature Geoscience*, 11(3), pp. 168–172. doi: 10.1038/s41561-018-0071-2.

Lee, S. H. *et al.* (2016) 'A statistical study of plasmaspheric plumes and ionospheric outflows observed at the dayside magnetopause', *Journal of Geophysical Research A: Space Physics*, 121(1), pp. 492–506. doi: 10.1002/2015JA021540.

Li, M., Zhong, S. and Olson, P. (2018) 'Linking lowermost mantle structure, core-mantle boundary heat flux and mantle plume formation', *Physics of the Earth and Planetary Interiors*, 277(August 2017), pp. 10–29. doi: 10.1016/j.pepi.2018.01.010.

Meert, J. G. *et al.* (2016) 'Rapid changes of magnetic Field polarity in the late Ediacaran: Linking the Cambrian evolutionary radiation and increased UV-B radiation', *Gondwana Research*, 34, pp. 149–157. doi: 10.1016/j.gr.2016.01.001.

- Merdith, A. S. *et al.* (2017) 'A full-plate global reconstruction of the Neoproterozoic', *Gondwana Research*, 50, pp. 84–134. doi: 10.1016/j.gr.2017.04.001.
- Mound, J. *et al.* (2019) 'Regional stratification at the top of Earth's core due to core–mantle boundary heat flux variations', *Nature Geoscience*, 12(7), pp. 575–580. doi: 10.1038/s41561-019-0381-z.
- Nakagawa, T. (2020) 'A coupled core-mantle evolution: review and future prospects', *Progress in Earth and Planetary Science*, 7(1). doi: 10.1186/s40645-020-00374-8.
- Nakagawa, T. and Tackley, P. J. (2008) 'Lateral variations in CMB heat flux and deep mantle seismic velocity caused by a thermal-chemical-phase boundary layer in 3D spherical convection', *Earth and Planetary Science Letters*, 271(1–4), pp. 348–358. doi: 10.1016/j.epsl.2008.04.013.
- Niu, Y. (2018) 'Origin of the LLSVPs at the base of the mantle is a consequence of plate tectonics – A petrological and geochemical perspective', *Geoscience Frontiers*, 9(5), pp. 1265–1278. doi: 10.1016/j.gsf.2018.03.005.
- Olson, P. *et al.* (2013) 'Controls on geomagnetic reversals and core evolution by mantle convection in the Phanerozoic', *Physics of the Earth and Planetary Interiors*, 214, pp. 87–103. doi: 10.1016/j.pepi.2012.10.003.
- Olson, P. and Amit, H. (2014) 'Magnetic reversal frequency scaling in dynamos with thermochemical convection', *Physics of the Earth and Planetary Interiors*, 229, pp. 122–133. doi: 10.1016/j.pepi.2014.01.009.
- Olson, P. and Christensen, U. R. (2002) 'The time-averaged magnetic field in numerical dynamos with non-uniform boundary heat flow', *Geophysical Journal International*, 151(3), pp.

809–823. doi: 10.1046/j.1365-246X.2002.01818.x.

Olson, P. L. *et al.* (2010) 'Geodynamo reversal frequency and heterogeneous core-mantle boundary heat flow', *Physics of the Earth and Planetary Interiors*, 180(1–2), pp. 66–79. doi: 10.1016/j.pepi.2010.02.010.

Oreskes, N., Shrader-Frechette, K. and Belitz, K. (1994) 'Verification, validation, and confirmation of numerical models in the earth sciences', *Science*, 263(5147), pp. 641–646. doi: 10.1126/science.263.5147.641.

Pavlov, V. and Gallet, Y. (2005) 'A third superchron during the Early Paleozoic', *Episodes*, 28(2), pp. 78–84. doi: 10.18814/epiiugs/2005/v28i2/001.

Robert, B., Greff-Lefftz, M. and Besse, J. (2018) 'True Polar Wander: A Key Indicator for Plate Configuration and Mantle Convection During the Late Neoproterozoic', *Geochemistry, Geophysics, Geosystems*, 19(9), pp. 3478–3495. doi: 10.1029/2018GC007490.

Steinberger, B. and Calderwood, A. R. (2006) 'Models of large-scale viscous flow in the Earth's mantle with constraints from mineral physics and surface observations', *Geophysical Journal International*, 167(3), pp. 1461–1481. doi: 10.1111/j.1365-246X.2006.03131.x.

Steinberger, B. and Torsvik, T. H. (2008) 'Absolute plate motions and true polar wander in the absence of hotspot tracks', *Nature*, 452(7187), pp. 620–623. doi: 10.1038/nature06824.

Terra-Nova, F., Amit, H. and Choblet, G. (2019) 'Preferred locations of weak surface field in numerical dynamos with heterogeneous core-mantle boundary heat flux: Consequences for the South Atlantic Anomaly', *Geophysical Journal International*, 217(2), pp. 1179–1199. doi: 10.1093/gji/ggy519.

- Thallner, D., Biggin, A. J. and Halls, H. C. (2021) 'An extended period of extremely weak geomagnetic field suggested by palaeointensities from the Ediacaran Grenville dykes (SE Canada)', *Earth and Planetary Science Letters*, 568, p. 117025. doi: 10.1016/j.epsl.2021.117025.
- Torsvik, T. H. *et al.* (2012) 'Phanerozoic Polar Wander, Palaeogeography and Dynamics', *Earth-Science Reviews*, 114(3–4), pp. 325–368. doi: 10.1016/j.earscirev.2012.06.007.
- Torsvik, T. H. *et al.* (2014) 'Deep mantle structure as a reference frame for movements in and on the Earth', *Proceedings of the National Academy of Sciences of the United States of America*, 111(24), pp. 8735–8740. doi: 10.1073/pnas.1318135111.
- Vilella, K. *et al.* (2021) 'Constraints on the composition and temperature of LLSVPs from seismic properties of lower mantle minerals', *Earth and Planetary Science Letters*, 554, p. 116685. doi: 10.1016/j.epsl.2020.116685.
- Wei-Jia Su, Woodward, R. L. and Dziewonski, A. M. (1994) 'Degree 12 model of shear velocity heterogeneity in the mantle', *Journal of Geophysical Research*, 99(B4), pp. 6945–6980. doi: 10.1029/93JB03408.
- Wei, Y. *et al.* (2014) 'Oxygen escape from the Earth during geomagnetic reversals: Implications to mass extinction', *Earth and Planetary Science Letters*, 394, pp. 94–98. doi: 10.1016/j.epsl.2014.03.018.
- Zhang, D. *et al.* (2021) 'Frequent Polarity Reversals in the Cretaceous Normal Superchron', *Geophysical Research Letters*, 48(5), pp. 1–13. doi: 10.1029/2020GL091501.
- Zhong, J. Q. and Zhang, J. (2005) 'Thermal convection with a freely moving top boundary', *Physics of Fluids*, 17(11), pp. 1–12. doi: 10.1063/1.2131924.

7 Appendix A

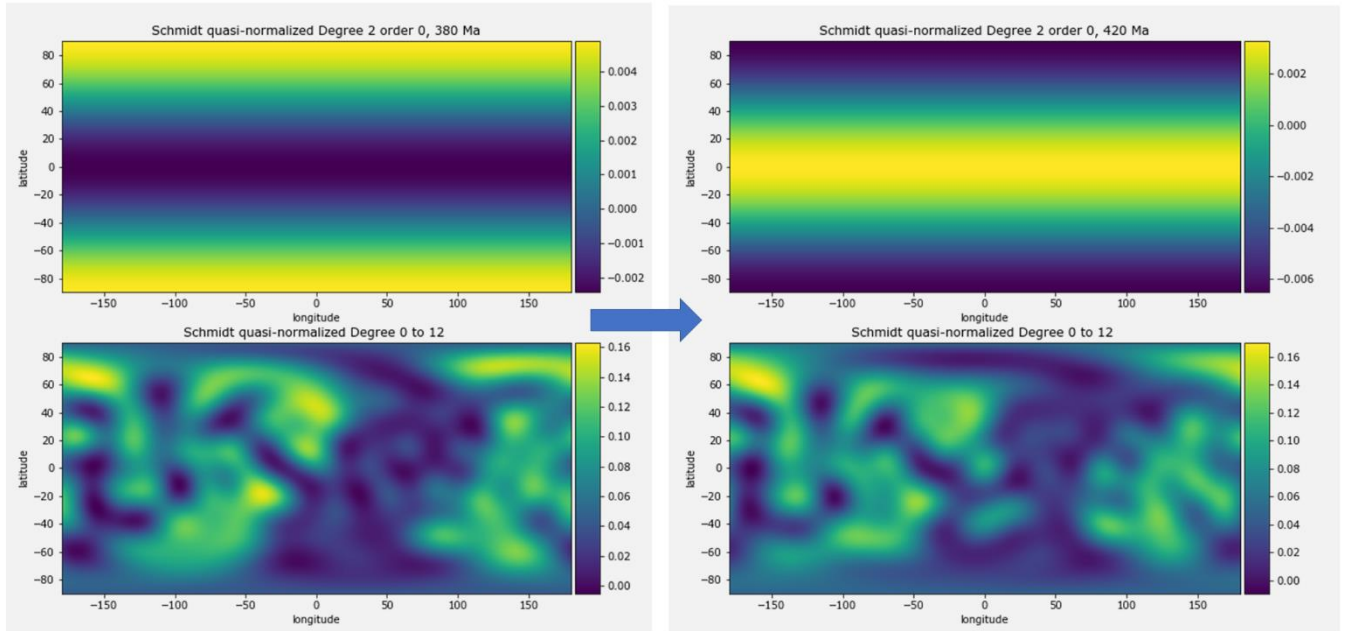


Figure A1. ‘flip’ CMB heat flux signal dominance derived from Case 1, flipping from polar regions to equatorial regions. Top panels contains the signal decomposed into degree two order zero spherical harmonics. Bottom panel displays the signal decomposed into spherical harmonic degrees 1 – 12.